Expert Systems With Applications 226 (2023) 120160

Contents lists available at ScienceDirect

Expert Systems With Applications

journal homepage: www.elsevier.com/locate/eswa

A machine learning approach to predict the k-coverage probability of wireless multihop networks considering boundary and shadowing effects

Jaiprakash Nagar [a,*], Sanjay Kumar Chaturvedi [a], Sieteng Soh [b], Abhilash Singh [c]

[a] Subir Chowdhury School of Quality and Reliability, Indian Institute of Technology Kharagpur, 721302, West Bengal, India
[b] School of Electrical Engineering, Computing and Mathematical Sciences, Curtin University, Perth WA 6102, Australia
[c] Fluvial Geomorphology and Remote Sensing Laboratory, Indian Institute of Science Education and Research Bhopal, 462066, Madhya Pradesh, India

ARTICLE INFO

Keywords:
Network k-coverage probability
Boundary effects
Shadowing effects
Machine learning algorithms
GRNN
Time complexity

ABSTRACT

Network coverage is a pivotal performance metric of wireless multihop networks (WMNs) determining the quality of service rendered by the network. Earlier, a few studies have analysed the network coverage by incorporating shadowing effects (SEs) and ignoring the influence of boundary effects (BEs). Besides, there is a void in the literature considering BEs plus SEs together. These approaches not only provide overestimation in network coverage, but also requires intensive simulation for their validation before the actual network installation; thus, increasing the computational time significantly. Furthermore, simulation time shoots up with an increase in network parameters like the number of sensor nodes (SNs) and their sensing range. In this study, we tackle this high simulation time problem by proposing a generalised regression neural network (GRNN) based machine learning (ML) approach to predict the k-coverage performance of a WMN placed in a rectangular-shaped region (RSR). To train the GRNN algorithm for two different set-ups, *i.e.*, without and with BEs, we extract six potential features, namely length of RSR, breadth of RSR, sensing range of SNs, number of SNs, standard deviation of SEs (σ), and the value required k through simulations. We also evaluate the importance of individual feature utilising regression tree ensemble technique and simultaneously analysed the sensitivity of each feature to predict the k-coverage probability of the network. The proposed approach has a better prediction accuracy of the k-coverage metric for both with and without BEs scenarios (having R = 0.78 and Root Mean Square Error (RMSE) = 0.14 for with BEs scenario, and R = 0.78 and RMSE = 0.15 for without BEs scenario). It can also be observed that the proposed approach achieves a higher accuracy with minimum computational time complexity as compared to other existing benchmark algorithms.

1. Introduction

Technological advancements in micro-electromechanical systems (MEMS) and wireless communication techniques have facilitated the manufacturing of tiny, energy-efficient, and low-cost micro-sensing devices with tremendous computational and functional capabilities. A WMN is made of an colossal number of small, low-powered, low-cost sensing devices possessing in-built sensing and wireless communication capabilities (Singh, Sharma, & Singh, 2021). Furthermore, these networks require no framework and work in a decentralised and self-organised fashion by exploiting single/multihop transmission over a wireless channel to transmit the gathered information to the intended receiver and communicate with the other sensing devices (Amutha, Sharma, & Sharma, 2021; Sharma & Nagar, 2020). Currently, WMNs are made of SNs with many in-built technologies like Global Positioning System (GPS) module, Infrared (IR) and thermal sensing modules with software, hardware, programming methodologies, and networking capabilities on a single chip. Hence they have an enormous number of applications, including border security, battlefield surveillance and reconnaissance, industrial automation and control, home automation, internet of things (IoT), telecommunication, healthcare applications, precision agriculture through soil moisture, environment monitoring, habitat monitoring, *etc* (Han et al., 2016; Kandris, Nakas, Vomvas, & Koulouras, 2020; Kotiyal, Singh, Sharma, Nagar, & Lee, 2021; Seferagić, Famaey, De Poorter, & Hoebeke, 2020; Singh, Gaurav, Meena, & Kumar, 2020; Stoyanova, Nikoloudakis, Panagiotakis, Pallis, & Markakis, 2020). In the rest of the paper, a network means a WMN.

The effective coverage area (ECA) of SNs installed close to the boundaries of the network region (NR) is less as compared with the ECA of SNs placed in the centre of the NR; this phenomenon is known

* Corresponding author.
E-mail addresses: jpnagar@iitkgp.ac.in (J. Nagar), skcrec@hijli.iitkgp.ac.in (S.K. Chaturvedi), s.soh@curtin.edu.au (S. Soh), sabhilash@iiserb.ac.in (A. Singh).

https://doi.org/10.1016/j.eswa.2023.120160
Received 14 November 2021; Received in revised form 21 March 2023; Accepted 14 April 2023
Available online 23 April 2023

Acronyms

WMNs	Wireless Multihop Networks
MEMS	Micro-Electromechanical Systems
WSNs	Wireless Sensor Networks
MIMO	Multiple-Input Multiple-Output
SNs	Sensor Nodes
GPS	Global Positioning System
2D	Two Dimensional
IR	Infrared
SEs	Shadowing Effects
IoT	Internet of Things
BEs	Boundary Effects
ML	Machine Learning
RSR	Rectangular Shaped Region
GRNN	Generalised Regression Neural Network
ECA	Effective Coverage Area
RMSE	Root Mean Square Error
RSSI	Received Signal Strength Indicator
ICE	Individual Conditional Expectation
NR	Network Region
PDP	Partial Dependence Plot

as boundary effects (BEs). The analytical models applicable for the coverage and connectivity analysis of the grand-scale networks are not usable for the limited small networks because an increase in the dimensions of the NR or the number of SNs can disrupt the linearity and dependencies between the variables and induce non-linearity in the network subtleties (Albert & Barabási, 2002; Brust, Ribeiro, & Barbosa Filho, 2009; Dalveren & Ali, 2020; Nze, Guinand, & Pigne, 2011; Pal et al., 2022). In addition to BEs, radio waves propagate through an environment full of impediments and susceptible to various phenomena such as interference, shadowing, fading, and multipath losses, *etc.*, taking place in the propagation environment. Furthermore, the existence of obstructions in the propagation environment and the increase in the separation between transmitter and receiver deteriorates the strength of the transmitted signal. Consequently, the received signal power fluctuates widely and rapidly, this deviation in received signal strength is called shadowing effects (SEs). It is imperative to consider both BEs and SEs together whilst deriving analytical solutions for the performance estimation of WMNs.

There exists an enormous literature which has examined the effect of environmental characteristics like interference, fading, shadowing, and multipath etcetera on the coverage performance of WMNs (Afshang & Dhillon, 2017; Al-Turjman, Hassanein, & Ibnkahla, 2013; Alam, Kamruzzaman, Karmakar, & Murshed, 2014; Amutha, Nagar, & Sharma, 2021; Debnath & Hossain, 2019; Fadoul, 2020; Hechmi, Zrelli, Kbida, Khlaifi, & Ezzedine, 2018; Miao, Huang, & Jia, 2020; Tsai, 2008). These works have significant contributions in characterising the coverage and connectivity performance of wireless network because one way or the other, they all have considered the environmental characteristics in their analysis. However, the major drawback of these studies have been to ignore the impact of BEs, a phenomenon affecting the performance of WMNs.

There exists a limited number of published work which has considered BEs in their models to estimate the coverage and connectivity metrics of WMNs (Habibiyan & Sabbagh, 2022; Khalid & Durrani, 2013; Laranjeira & Rodrigues, 2014; Liu, Jia, & Wang, 2018; Nagar, Chaturvedi, & Soh, 2020a). These studies have provided a deep insight of the influence of BEs on wireless networks performance, but, they have assumed a disk based transmission range model. The models proposed in these studies assumed a constant transmission range of SNs in all directions which is neither appropriate nor observed.

Despite the fact that the above-mentioned models perform well for the analysis of network performance, however, these approaches require intensive simulations for their validation before the network set-up. For example, the analytical model for the k-connectivity of the network provided in Laranjeira and Rodrigues (2014) is validated through MCS exhibiting high computational time, *i.e.*, time taken to get one single simulation result at a specified value of number of nodes, sensing range, and 10000 iterations is more than fifteen hours. Other examples could be seen in Khalid and Durrani (2013), Nagar et al. (2020a) have also employed the MCS methods to substantiate their proposed analytical solutions having high time complexity.

Further, it is important to mention that an increase in SN's count also increases the computational cost and time exponentially. To minimise the computational time and cost of MCS for the type of problem we are addressing, one of the alternative way is to employ ML based approaches. It is well-known that in many of the complex problems, ML approaches have reduced the time from hours to even seconds and predicted the results close to the results estimated by computationally intensive algorithms. Hence, ML approaches provides fast and accurate estimation of network performance metrics (Singh, Nagar, Sharma, & Kotiyal, 2021).

Broadly, ML approaches are classified into two categories; unsupervised and supervised learning approaches. Supervised learning approaches operate with label datasets whereas unsupervised learning approaches work with unlabelled datasets. Further, supervised learning approaches are divided into classification and regression task. A brief surveys on ML based approaches for WSNs, strategies, and applications can be seen in Alsheikh, Lin, Niyato, and Tan (2014), Chen, Challita, Saad, Yin, and Debbah (2019), Kumar, Amgoth, and Annavarapu (2019). Currently, ML based approaches are being used for various WSN applications such as target tracking (Mahfouz, Mourad-Chehade, Honeine, Farah, & Snoussi, 2014), intrusion detection (Kang & Kang, 2016; Singh, Nagar, et al., 2021; Tan et al., 2019), anomaly detection (Mamun, Islam, & Kaosar, 2014) network connectivity (Stern, Song, & Work, 2017), path loss prediction (Jo, Park, Lee, Choi, & Park, 2020), coverage estimation in mobile networks (Fernandes et al., 2020), routing in WSN (Nayak, Swetha, Gupta, & Madhavi, 2021), remote sensing (Singh, Gaurav, Rai, & Beg, 2021), earth science (Kamel, Afan, Sherif, Ahmed, & El-Shafie, 2021), block chain driven IoT (Internet of Things) (Chowdhury, Rahman, Rahman, & Mahdy, 2020; Jeong & Sim, 2021), smart cities (Sharma, Haque, & Blaabjerg, 2021), average localisation error (Singh, Kotiyal, Sharma, Nagar, & Lee, 2020) and many others. In addition to WSNs, ML based approaches are also being employed in cellular networks, advanced and next-generation networks (5G and 6G) (Ali et al., 2020; Du, Jiang, Wang, Ren, & Debbah, 2020; Fourati, Maaloul, & Chaari, 2021; Jiang et al., 2016) for smart grid, device-to device communications, femto/small cells, massive MIMOs, heterogeneous networks, cognitive radios, energy harvesting, connectivity and vehicular traffic prediction (Ide et al., 2015), radio coverage prediction (Mohammadjafari et al., 2020), optimisation of coverage and capacity (Dreifuerst et al., 2021), and so on.

GRNN is a supervised regression based ML method which can train in almost no time using a limited training data set. In addition, it has a non-iterative and highly parallel neural architecture. Earlier, Rahman, Park, and Kim (2012) provided a location evaluation algorithms using GRNN and weighted centroid localisation. They used RSS data to train the proposed model and then estimated the target position in its close neighbours. Recently, the authors in Jondhale and Deshpande (2018) proposed two GRNN based algorithms named GRNN + KF and GRNN + UKF to compute the location of single target mobile in 2-D in WSN. The same authors in Jondhale and Deshpande (2019) also proposed a GRNN-based localisation approach which uses RSSI measurements in large scale wheat farmland to locate the target. Most recently, Vijayakumar and Balakrishnan (2021) proposed a GRNN-based ML algorithm to analyse agriculture monitoring data that can be used for automation. They tested several ML algorithms and found that among all tested algorithms GRNN is best suited for the task in hand. However, GRNN based ML approach has not been applied for the coverage estimation of WMN.

In this study, we propose an ML based technique to map the k-coverage probability of a WMN with minimum computational time requirements. We present a GRNN based ML approach on the simulated data to predict the k-coverage performance considering SEs for two different scenarios; with and without BEs. We extract six different features, namely length of RSR, breadth of RSR, sensing range of SNs, number of SNs, standard deviation of SEs (σ), and the value of k required. Eventually, we have trained the GRNN algorithm using these features and evaluated its performance using R, RMSE, bias and computational time complexity as the performance metrics. To the best of our awareness, no other research has been conducted and publicised to tackle this issue through ML approach. The key contributions of this research are listed below.

1. First, we develop an analytical model incorporating BEs only, and then BEs plus SEs together to evaluate the k-coverage probability of a finite WMN spread in a finite RSR.
2. Secondly, we extract potential features through MCS and evaluated their relative importance, and sensitivity in estimating the k-coverage metric of the WMN.
3. Lastly, we applied GRNN ML algorithm to evaluate the k-coverage performance of the WMN speedily and accurately.

The remaining of the paper is organised as follows: The SN's distribution model, sensing range models, and some coverage related definitions are rendered in Section 2. We explained our analytical model to compute the ECA of an SN in various boundary and non-boundary regions using considered sensing range models in Section 3. Further, an ML based approach to predict the k-coverage probability of the WMN is discussed in Section 4. Results of the proposed ML based approach for with and without BEs scenarios are given and studied in Section 5 and Section 6 respectively. Finally, Section 7 concludes the paper.

2. System model

Existing literature assumed different finite geometrical shapes like a convex-shaped polygons (Gupta, Rao, & Venkatesh, 2014), a circle (Arora & Pal, 2022), a square (Katti, 2022), and a hexagon (Xu & Lin, 2023). However, in this study, we assumed a finite RSR. The main advantage of using an RSR is that a generalised RSR can be used as a reference to derive analytical models for other shaped regions. For instance, we can quickly obtain results for finite square regions by simply considering equal length and width. Further, a generalised RSR can be used as a reference to derive analytical models for other shaped areas.

Here below, we briefly describe the SN distribution model, pertinent sensing range models, coverage-related terms and definitions, and some difficulties in evaluating the target detection probability in different sub-regions of a RSR. Without the loss of generality, let all SNs are homogeneous, *i.e.*, each SN possesses the equal amount of energy, computational, sensing, and transmission capabilities.

- **Sensor Node Distribution Model**: A static WMN is assumed to be made by distributing N number of SNs independently and uniformly (*i.e.*, probability of lying onto any spot within the region is equal for each SN) inside a finite RSR $\mathfrak{R}$ of length $'l'$ meters by width $'w'$ meters. The location of an SN in the region is denoted by $P(x, y)$.

$$\{P(x,y) \in \mathfrak{R} | 0 \le x \le l, 0 \le y \le w\} \tag{1}$$

- **Sensing Range Models**: In this work, we presume two most widely employed sensing range models discussed briefly below.
  - *Circular disk sensing range model* is widely employed for deriving analytical solutions and evaluating the efficacy of WMNs (Khalid & Durrani, 2013; Laranjeira & Rodrigues, 2014; Nagar et al., 2020a). A target is assumed to be detected by an SN if it is positioned within any SN's sensing range. Mathematically, it can be rendered by Eq. (2)

$$P_{det}(r) = \begin{cases} 1, r \le r_{max} \\ 0, r > r_{max} \end{cases} \tag{2}$$

    This model considers a identical sensing range for all the possible directions, which is not valid because most of the signals are affected by impediments present in the propagation path, noise, radio fluctuations, interference, multipath fading, reflection, and refraction *etc.,* (Amutha, Sharma, & Nagar, 2020; Nagar, Chaturvedi, & Soh, 2020b; Tsai, 2008). Therefore, it is not suitable for practical applications. To overcome the constraints of the circular disk sensing range model, we consider another sensing range model named the Log-normal shadowing path loss model.
  - *The Log-normal shadowing path loss model*: This model addresses the shortcomings of the circular disk sensing range model. We can utilise this model to characterise the signal propagation in realistic environments. In addition, the existence of obstructions in signal propagation environment causes shadowing and fading effects along with the path loss due to the disperse of signal power radiated by the transmitter. Additionally, the detection ability of SNs diminishes with the increase in distance of target or event from the SNs. Thus, the sensing range of SNs is not fixed in every directions and depends on shadowing in different directions. Now, assume that the location of a target or an event is r units distant from the SN, then the probability that the target or the event would be detected by the SN is given by Eq. (3) (Tsai, 2008)

$$P_{det}(r) = \phi\left(\frac{10\beta \log_{10}(r/\bar{r})}{\sigma}\right) \tag{3}$$

    where, $\phi(\psi) = \frac{1}{\sqrt{2\pi}} \int_{\psi}^{\infty} \exp\left(\frac{-\chi_\sigma^2}{2}\right) d\chi_\sigma$; β, σ and $\bar{r}$ represent the signal power decay factor, standard deviation of SEs, and the expected sensing range of SNs respectively.

3. Target detection probabilities for network k-coverage

This section derives the various expressions incorporating only BEs and BEs plus SEs together to calculate the k-coverage metric of a WMN.

3.1. Target detection probability with BEs only

The probability that a target in the RSR would be sensed by a uniformly and randomly distributed SN positioned at a random location P within the RSR is represented by the overlapping area $|A(P; r_{max}) \cap R| / (l \times w)$. The effective obvoluting area of an SN is calculated by dividing the whole RSR into various sub-regions such as inner sub-region denoted by I, lateral boundary sub-regions denoted by B_1, B_2, B_3, and B_4, inner corner sub-regions denoted by C_{I1}, C_{I2}, C_{I3}, and C_{I4}, and outer corner sub-regions denoted by C_{O1}, C_{O2}, C_{O3}, and C_{O4}, respectively as shown in Fig. 1.

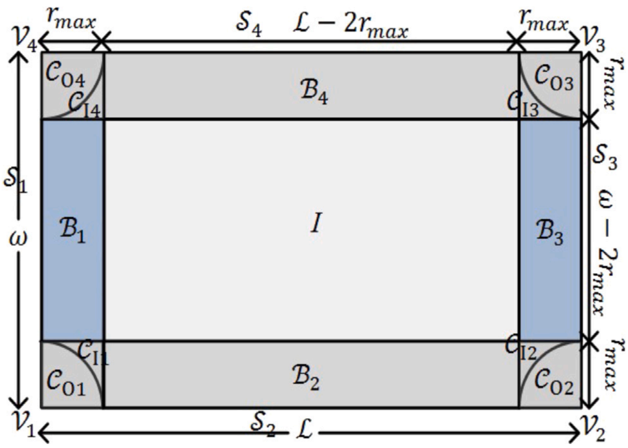

Fig. 1. Different sub-regions of an RSR.

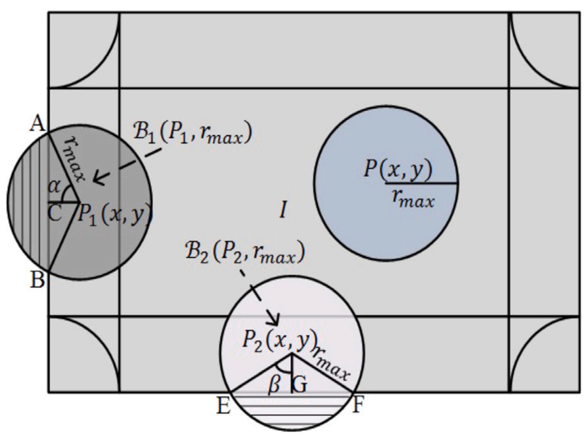

Fig. 2. ECA of an SN in I, B_1, and B_2.

3.1.1. Target detection probability of an SN placed in inner sub-region I

This probability can be represented and calculated in the following manner. Let there be an SN is lying at an arbitrary location denoted by $P(x, y)$ in sub-region I of the RSR as shown in Fig. 2. We observe that the coverage area of an SN does not suffer any kind of BEs in I, therefore, the ECA of the SN is equal to πr_{max}^2. Consequently, the probability that a random target position inside the RSR would be detected by an SN lying in I is computed as

$$P_{det}^{I} = \frac{\pi r_{max}^2}{l \times w} \tag{4}$$

3.1.2. Target detection probability of an SN placed in lateral boundary sub-regions

Suppose that a arbitrary SN is positioned at a location P_1 within the lateral boundary sub-region B_1. In this case, the ECA of an SN is not equal to πr_{max}^2 because some area of the SN falls outside the side S_1 of the RSR as shown in Fig. 2. The ECA of the SN placed at P_1 is denoted by $A(B_1)$ and is obtained by deducting the area of the circular part emerged beyond side S_1 from the circular disk area πr_{max}^2. The area of the circular part emerged beyond side S_1 is computed by subtracting the triangular section area from the circular part area, thus

$$area\left(\widehat{ABP_1}\right) = r_{max}^2 cos^{-1}\left(\frac{x}{r_{max}}\right) \tag{5}$$

$$area\left(\Delta AP_1B\right) = x\sqrt{r_{max}^2 - x} \tag{6}$$

and the area of the circular part emerged beyond side S_1 will be

$$\begin{aligned} area\left(\widehat{ABA}\right) &= area\left(\widehat{ABP_1}\right) - area\left(\Delta AP_1B\right) \\ &= r_{max}^2 cos^{-1}\left(\frac{x}{r_{max}}\right) - x\sqrt{r_{max}^2 - x^2} \end{aligned} \tag{7}$$

Thus, the ECA of the SN lying inside sub-region B_1 is given by

$$\begin{aligned} A\left(B_1\right) &= \pi r_{max}^2 - area\left(\widehat{ABA}\right) \\ &= \pi r_{max}^2 - r_{max}^2 cos^{-1}\left(\frac{x}{r_{max}}\right) + x\sqrt{r_{max}^2 - x^2} \end{aligned} \tag{8}$$

Similarly, the ECA of an SN in sub-regions B_2, B_3, and B_4 are denoted by $A(B_2), A(B_3)$, and $A(B_4)$, respectively and can be calculated using Eq. (9) to Eq. (11).

$$A\left(B_2\right) = \pi r_{max}^2 - r_{max}^2 cos^{-1}\left(\frac{y}{r_{max}}\right) + y\sqrt{r_{max}^2 - y^2} \tag{9}$$

$$A\left(B_3\right) = \pi r_{max}^2 - r_{max}^2 cos^{-1}\left(\frac{l-x}{r_{max}}\right) + (l-x)\sqrt{r_{max}^2 - (l-x)^2} \tag{10}$$

$$A\left(B_4\right) = \pi r_{max}^2 - r_{max}^2 cos^{-1}\left(\frac{w-y}{r_{max}}\right) + (w-y)\sqrt{r_{max}^2 - (w-y)^2} \tag{11}$$

The probability that an arbitrary target position within the RSR would be sensed by an SN positioned in sub-region B_1 is calculated as

$$P_{det}^{B_1} = \frac{A\left(B_1\right)}{l \times w} = \frac{\pi r_{max}^2 - r_{max}^2 cos^{-1}\left(\frac{x}{r_{max}}\right) + x\sqrt{r_{max}^2 - x^2}}{l \times w} \tag{12}$$

Furthermore, the probability that an arbitrary target location would be sensed by an SN lying in sub-regions B_2, B_3, and B_4 is calculated using Eq. (13), Eq. (14) and (15), respectively

$$P_{det}^{B_2} = \frac{A\left(B_2\right)}{l \times w} = \frac{\pi r_{max}^2 - r_{max}^2 cos^{-1}\left(\frac{y}{r_{max}}\right) + y\sqrt{r_{max}^2 - y^2}}{l \times w} \tag{13}$$

$$P_{det}^{B_3} = \frac{A\left(B_3\right)}{l \times w} = \frac{\pi r_{max}^2 - r_{max}^2 cos^{-1}\left(\frac{l-x}{r_{max}}\right) + (l-x)\sqrt{r_{max}^2 - (l-x)^2}}{l \times w} \tag{14}$$

$$P_{det}^{B_4} = \frac{A\left(B_4\right)}{l \times w} = \frac{\pi r_{max}^2 - r_{max}^2 cos^{-1}\left(\frac{w-y}{r_{max}}\right) + (w-y)\sqrt{r_{max}^2 - (w-y)^2}}{l \times w} \tag{15}$$

Further, it is noteworthy that the expected ECA and the target detection probability of an arbitrary SN placed in sub-regions B_1 and B_2 are equal to the expected ECA and target detection probability of the SN positioned in sub-region B_3 and B_4 respectively due to the symmetry of these sub-regions.

3.1.3. Target detection probability of an SN placed in inner corner sub-regions

Here, we presume that an arbitrary SN is positioned at a location P in inner corner sub-region C_{I1}. When the SN is lying in sub-region C_{I1}, some of its coverage area falls outside the sides' S_1 and S_2 as shown in Fig. 3. Thus, the ECA of the SN positioned in inner corner C_{I1} is not equal to πr_{max}^2, and is obtained by deducting the area of two circular parts emerged beyond S_1 and S_2 from the circular disk area πr_{max}^2. The area of both the circular segments is calculated in a similar manner as we calculated $A(B_1)$. Therefore, we get

$$\begin{aligned} area\left(\widehat{AB}\right) &= area\left(\widehat{ABP}\right) - area\left(\Delta APB\right) \\ &= r_{max}^2 cos^{-1}\left(\frac{x}{r_{max}}\right) - x\sqrt{r_{max}^2 - x^2} \end{aligned} \tag{16}$$

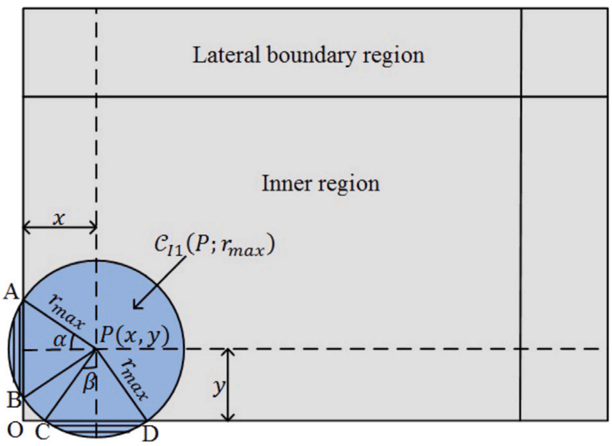

Fig. 3. ECA of an SN in sub-region C_{I1}.

and

$$area\left(\widehat{CD}\right) = area\left(\widehat{CDP}\right) - area\left(\Delta CPD\right) = r_{max}^2 cos^{-1}\left(\frac{y}{r_{max}}\right) - y\sqrt{r_{max}^2 - y^2} \tag{17}$$

Consequently, the ECA of an SN positioned in sub-region C_{I1} denoted by $A\left(C_{I1}\right)$ is obtained as

$$\begin{aligned} A\left(C_{I1}\right) &= \pi r_{max}^2 - area\left(\widehat{AB}\right) - area\left(\widehat{CD}\right) \\ &= \pi r_{max}^2 - r_{max}^2 cos^{-1}\left(\frac{x}{r_{max}}\right) - r_{max}^2 cos^{-1}\left(\frac{y}{r_{max}}\right) \\ &\quad + x\sqrt{r_{max}^2 - x^2} + y\sqrt{r_{max}^2 - y^2} \end{aligned} \tag{18}$$

Similarly, the ECA of an SN in sub-regions C_{I2}, C_{I3}, and C_{I4} is denoted by $A\left(C_{I2}\right)$, $A\left(C_{I3}\right)$, and $A\left(C_{I4}\right)$, respectively and is calculated using Eq. (19) to Eq. (21):

$$\begin{aligned} A\left(C_{I2}\right) &= \pi r_{max}^2 - r_{max}^2 cos^{-1}\left(\frac{l-x}{r_{max}}\right) - r_{max}^2 cos^{-1}\left(\frac{y}{r_{max}}\right) \\ &\quad + (l-x)\sqrt{r_{max}^2 - (l-x)^2} + y\sqrt{r_{max}^2 - y^2} \end{aligned} \tag{19}$$

$$\begin{aligned} A\left(C_{I3}\right) &= \pi r_{max}^2 - r_{max}^2 cos^{-1}\left(\frac{l-x}{r_{max}}\right) - r_{max}^2 cos^{-1}\left(\frac{l-y}{r_{max}}\right) \\ &\quad + (l-x)\sqrt{r_{max}^2 - (l-x)^2} + (w-y)\sqrt{r_{max}^2 - (w-y)^2} \end{aligned} \tag{20}$$

$$\begin{aligned} A\left(C_{I4}\right) &= \pi r_{max}^2 - r_{max}^2 cos^{-1}\left(\frac{x}{r_{max}}\right) - r_{max}^2 cos^{-1}\left(\frac{w-y}{r_{max}}\right) \\ &\quad + x\sqrt{r_{max}^2 - x^2} + (w-y)\sqrt{r_{max}^2 - (w-y)^2} \end{aligned} \tag{21}$$

The probability that an arbitrary target position in the RSR would be sensed by an SN positioned in sub-region C_{I1} is calculated as

$$P_{det}^{C_{I1}} = \frac{A\left(C_{I1}\right)}{A} = \frac{\pi r_{max}^2 - r_{max}^2 cos^{-1}\left(\frac{x}{r_{max}}\right) - r_{max}^2 cos^{-1}\left(\frac{y}{r_{max}}\right) + x\sqrt{r_{max}^2 - x^2} + y\sqrt{r_{max}^2 - y^2}}{A} \tag{22}$$

Furthermore, the probability that an arbitrary target location would be sensed by an SN lying in sub-regions C_{I2}, C_{I3}, and C_{I4} is calculated using Eq. (23), Eq. (24), and Eq. (25), respectively

$$P_{det}^{C_{I2}} = \frac{A\left(C_{I2}\right)}{A} = \frac{\pi r_{max}^2 - r_{max}^2 cos^{-1}\left(\frac{l-x}{r_{max}}\right) - r_{max}^2 cos^{-1}\left(\frac{y}{r_{max}}\right)}{A} + \frac{(l-x)\sqrt{r_{max}^2 - (l-x)^2} + y\sqrt{r_{max}^2 - y^2}}{A} \tag{23}$$

$$P_{det}^{C_{I3}} = \frac{A\left(C_{I3}\right)}{A} = \frac{\pi r_{max}^2 - r_{max}^2 cos^{-1}\left(\frac{l-x}{r_{max}}\right) - r_{max}^2 cos^{-1}\left(\frac{l-y}{r_{max}}\right)}{A} + \frac{(l-x)\sqrt{r_{max}^2 - (l-x)^2} + (w-y)\sqrt{r_{max}^2 - (w-y)^2}}{A} \tag{24}$$

$$P_{det}^{C_{I4}} = \frac{A\left(C_{I4}\right)}{A} = \frac{\pi r_{max}^2 - r_{max}^2 cos^{-1}\left(\frac{x}{r_{max}}\right) - r_{max}^2 cos^{-1}\left(\frac{w-y}{r_{max}}\right)}{A} + \frac{x\sqrt{r_{max}^2 - x^2} + (w-y)\sqrt{r_{max}^2 - (w-y)^2}}{A} \tag{25}$$

It is noteworthy that the mean ECA of an SN in individual inner corner sub-region will be equal because of the symmetry of the RSR; as a result, the probability of arbitrary target position detection will also be equal in every inner corner sub-region.

3.1.4. Target detection probability of an SN placed in outer corner sub-regions

Assuming that an SN is placed at a position P in outer corner sub-region C_{O1} and its ECA is denoted by $A\left(C_{O1}\right)$. In this case, some coverage area of the SN falls outside the sides' S_1, S_2 and vertex V_1 as shown in Fig. 4. Therefore, ECA of the SN is less than πr_{max}^2, and is obtained by summing the area of the rectangular region OGPH as well as the area of three sectors *viz.*, sector $\widehat{BFP}$, sector $\widehat{BCP}$, and sector $\widehat{CEP}$ as depicted in Fig. 4. The entire area of sector $\widehat{BCP}$ falls within the RSR. However, some area of sectors $\widehat{BFP}$ and $\widehat{CEP}$ lie outside the RSR, thus, it is necessary to subtract these areas from their respective sector areas, we get

$$area\left(OGPH\right) = xy, \tag{26}$$

$$area\left(\widehat{BCP} + \widehat{BFP} + \widehat{CEP}\right) = \frac{3}{4}\pi r_{max}^2 \tag{27}$$

The area of sectors $\widehat{BFP}$ and $\widehat{CEP}$ lying outside the network region are computed as follows:

The area of sector $\widehat{BFP}$ lying outside the network region will be equal to the Area $\left(\widehat{AFP}\right)$ - Area(ΔAHP) and is given by

$$Area\left(\widehat{AFP}\right) - Area\left(\Delta AHP\right) = \frac{\pi r_{max}^2}{2} cos^{-1}\left(\frac{x}{r_{max}}\right) - \frac{x}{2}\sqrt{r_{max}^2 - x^2} \tag{28}$$

Similarly, the Area$\left(\widehat{CEP}\right)$ lying outside the network region is calculated using Eq. (29)

$$Area\left(\widehat{DEP}\right) - Area\left(\Delta DGP\right) = \frac{\pi r_{max}^2}{2} cos^{-1}\left(\frac{y}{r_{max}}\right) - \frac{y}{2}\sqrt{r_{max}^2 - y^2} \tag{29}$$

Therefore, the ECA $A\left(C_{O1}\right)$ of an SN in outer corner sub-region $\left(C_{O1}\right)$ of a RSR will be

$$\begin{aligned} A\left(C_{O1}\right) &= xy + \frac{3}{4}\pi r_{max}^2 - \frac{r_{max}^2}{2} cos^{-1}\left(\frac{x}{r_{max}}\right) - \frac{r_{max}^2}{2} cos^{-1}\left(\frac{y}{r_{max}}\right) \\ &\quad + \frac{x}{2}\sqrt{r_{max}^2 - x^2} + \frac{y}{2}\sqrt{r_{max}^2 - y^2} \end{aligned} \tag{30}$$

Likewise, the ECA of an SN in outer corner sub-regions C_{O2}, C_{O3}, and C_{O4} are denoted by $A\left(C_{O2}\right)$, $A\left(C_{O3}\right)$ and $A\left(C_{O4}\right)$ respectively, and

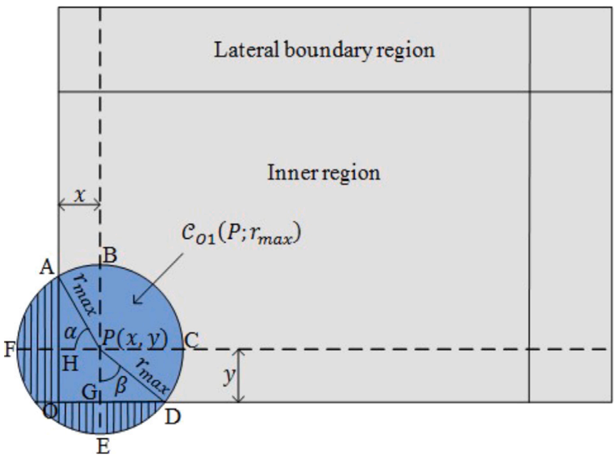

Fig. 4. ECA of an SN in sub-region C_{O1}.

can be calculated in a similar manner using Eq. (31) to Eq. (33)

$$A\left(C_{O2}\right) = (l-x)\,y + \frac{3}{4}\pi r_{max}^2 - \frac{r_{max}^2}{2} cos^{-1}\left(\frac{l-x}{r_{max}}\right) - \frac{r_{max}^2}{2} cos^{-1}\left(\frac{y}{r_{max}}\right) + \frac{(l-x)}{2}\sqrt{r_{max}^2-(l-x)^2} + \frac{y}{2}\sqrt{r_{max}^2-y^2} \tag{31}$$

$$A\left(C_{O3}\right) = (l-x)(w-y) + \frac{3}{4}\pi r_{max}^2 - \frac{r_{max}^2}{2} cos^{-1}\left(\frac{l-x}{r_{max}}\right) - \frac{r_{max}^2}{2} cos^{-1}\left(\frac{w-y}{r_{max}}\right) + \frac{(l-x)}{2}\sqrt{r_{max}^2-(l-x)^2} + \frac{(w-y)}{2}\sqrt{r_{max}^2-(w-y)^2} \tag{32}$$

$$A\left(C_{O4}\right) = x\,(w-y) + \frac{3}{4}\pi r_{max}^2 - \frac{r_{max}^2}{2} cos^{-1}\left(\frac{x}{r_{max}}\right) - \frac{r_{max}^2}{2} cos^{-1}\left(\frac{w-y}{r_{max}}\right) + \frac{x}{2}\sqrt{r_{max}^2-x^2} + \frac{(w-y)}{2}\sqrt{r_{max}^2-(w-y)^2} \tag{33}$$

The probability that an arbitrary target position inside the RSR would be detected by an SN lying in sub-region C_{O1} is calculated as

$$P_{det}^{C_{O1}} = \frac{xy + \frac{3}{4}\pi r_{max}^2 - \frac{r_{max}^2}{2} cos^{-1}\left(\frac{x}{r_{max}}\right) - \frac{r_{max}^2}{2} cos^{-1}\left(\frac{y}{r_{max}}\right)}{A} + \frac{\frac{x}{2}\sqrt{r_{max}^2-x^2} + \frac{y}{2}\sqrt{r_{max}^2-y^2}}{A} \tag{34}$$

and, the probability that an arbitrary target location would be sensed by an arbitrary SN lying in sub-regions C_{O2}, C_{O3}, and C_{O4} is calculated using Eq. (35), Eq. (36) and (37), respectively

$$P_{det}^{C_{O2}} = \frac{(l-x)\,y + \frac{3}{4}\pi r_{max}^2 - \frac{r_{max}^2}{2} cos^{-1}\left(\frac{l-x}{r_{max}}\right) - \frac{r_{max}^2}{2} cos^{-1}\left(\frac{y}{r_{max}}\right)}{A} + \frac{+\frac{(l-x)}{2}\sqrt{r_{max}^2-(l-x)^2} + \frac{y}{2}\sqrt{r_{max}^2-y^2}}{A} \tag{35}$$

$$P_{det}^{C_{O3}} = \frac{(l-x)(w-y) + \frac{3}{4}\pi r_{max}^2 - \frac{r_{max}^2}{2} cos^{-1}\left(\frac{l-x}{r_{max}}\right) - \frac{r_{max}^2}{2} cos^{-1}\left(\frac{(w-y)}{r_{max}}\right)}{A} + \frac{\frac{(l-x)}{2}\sqrt{r_{max}^2-(l-x)^2} + \frac{(w-y)}{2}\sqrt{r_{max}^2-(w-y)^2}}{A} \tag{36}$$

$$P_{det}^{C_{O4}} = \frac{x\,(w-y) + \frac{3}{4}\pi r_{max}^2 - \frac{r_{max}^2}{2} cos^{-1}\left(\frac{x}{r_{max}}\right) - \frac{r_{max}^2}{2} cos^{-1}\left(\frac{w-y}{r_{max}}\right)}{A} + \frac{\frac{x}{2}\sqrt{r_{max}^2-x^2} + \frac{(w-y)}{2}\sqrt{r_{max}^2-(w-y)^2}}{A} \tag{37}$$

It is necessary to mention that the mean ECA of an SN in individual outer corner sub-region will be same because of the symmetry of the RSR; as a result, the probability of an arbitrary target position detection will also be equal.

Now, we average the target detection probability of an SN over different sub-regions by considering BEs to estimate the expected probability of target detection by an arbitrary SN deployed inside the RSR

$$\begin{aligned} E\left(P_{det}\right) = & \int_{r_{max}}^{w-r_{max}} \int_{r_{max}}^{l-r_{max}} \left(\frac{P_{det}^{I}}{A}\right) dx\,dy \\ & + 2\int_{r_{max}}^{w-r_{max}} \int_{0}^{r_{max}} \left(\frac{P_{det}^{B_1}}{A}\right) dx\,dy \\ & + 2\int_{0}^{r_{max}} \int_{r_{max}}^{l-r_{max}} \left(\frac{P_{det}^{B_2}}{A}\right) dx\,dy \\ & + 4\int_{\sqrt{r_{max}^2-x^2}}^{r_{max}} \int_{0}^{r_{max}} \left(\frac{P_{det}^{C_{I1}}}{A}\right) dx\,dy \\ & + 4\int_{x}^{\sqrt{r_{max}^2-x^2}} \int_{0}^{r_{max}} \left(\frac{P_{det}^{C_{O1}}}{A}\right) dx\,dy \end{aligned} \tag{38}$$

3.2. Target detection probability with BEs and SEs

In this part, we explain the analytical formulation for k-coverage probability considering BEs and SEs concurrently.

3.2.1. Target detection probability of an SN placed in sub-region I

The probability calculation under this case is based on the premise that the coverage area of an arbitrary SN, lying in the inner sub-region I, does not experience BEs because of its position far from the boundaries of the RSR. The probability that the SN is located at a position with separation r to the target location is $2\pi r/A \times dr$, where dr is a tiny difference in separation as shown in Fig. 5. Thus, the probability that the target position would be sensed by this arbitrary SN is calculated as

$$\begin{aligned} P_{det}^{I}(r) &= \int_{0}^{r_{max}} P_{det}(r) \times \frac{2\pi r}{A}\,dr \\ &= \int_{0}^{r_{max}} \phi\left(\frac{10\beta \log_{10}(r/\bar{r})}{\sigma}\right) \times \frac{2\pi r}{A}\,dr \end{aligned} \tag{39}$$

3.2.2. Target detection probability of an SN placed in sub-region B_1

Assuming that an arbitrary SN is deployed at a random location in sub-region B_1 of the RSR, the coverage area of this arbitrary SN is limited by side S_1. Thus, the probability that the target is positioned at a point with separation r to the

SN location is $2\pi r \times dr/A$, $r \in [0, x]$ and $2r\left(\pi - cos^{-1}(x/r)\right) \times dr/A$, $r \in [x, r_{max}]$, where dr is a minute deviation in separation and can be computed with the help of Fig. 6. Thus, the probability that the target would be sensed by this arbitrary SN is computed as

$$\begin{aligned} P_{det}^{B_1}(r) &= \int_{0}^{x} \phi\left(\frac{10\beta \log_{10}(r/\bar{r})}{\sigma}\right) \times \frac{2\pi r}{A}\,dr \\ &\quad + \int_{x}^{r_{max}} \phi\left(\frac{10\beta \log_{10}(r/\bar{r})}{\sigma}\right) \times \frac{2r\left(\pi - cos^{-1}(x/r)\right)}{A}\,dr \\ &= \int_{0}^{r_{max}} \phi\left(\frac{10\beta \log_{10}(r/\bar{r})}{\sigma}\right) \times \frac{2\pi r}{A}\,dr \\ &\quad - \int_{x}^{r_{max}} \phi\left(\frac{10\beta \log_{10}(r/\bar{r})}{\sigma}\right) \times \frac{2r cos^{-1}(x/r)}{A}\,dr \end{aligned} \tag{40}$$

Note that in a shadowing environment, the probability that a target would be sensed by an arbitrary SN lying in lateral boundary sub-regions B_1 and B_3 will be equal because of the symmetry of the RSR.

3.2.3. Target detection probability of an SN placed in sub-region B_2

It is presumed that an arbitrary SN is placed at a position in sub-region B_2 of the RSR where the coverage area of the SN is limited by side S_2. Therefore, the probability that the target is lying at a location with separation r to SN position is $2\pi r \times dr/A$, $r \in [0, y]$ and $2r\left(\pi - cos^{-1}(y/r)\right) \times dr/A$, $r \in [y, r_{max}]$, where dr is a tiny difference in separation and can be computed with the help of Fig. 6. Thus, the probability that the target would be sensed by this arbitrary SN is computed as

$$\begin{aligned} P_{det}^{B_2}(r) &= \int_0^y \phi\left(\frac{10\beta \log_{10}(r/\bar{r})}{\sigma}\right) \times \frac{2\pi r}{A}\,dr \\ &+ \int_y^{r_{max}} \phi\left(\frac{10\beta \log_{10}\left(\frac{r}{\bar{r}}\right)}{\sigma}\right) \times \frac{2r\left(\pi - cos^{-1}(y/r)\right)}{A}\,dr \\ &= \int_0^{r_{max}} \phi\left(\frac{10\beta \log_{10}(r/\bar{r})}{\sigma}\right) \times \frac{2\pi r}{A}\,dr \\ &- \int_y^{r_{max}} \phi\left(\frac{10\beta \log_{10}(r/\bar{r})}{\sigma}\right) \times \frac{2r cos^{-1}(y/r)}{A}\,dr \end{aligned} \tag{41}$$

Similar to B_1 and B_3, the probability that a target would be sensed by an arbitrary SN lying in lateral boundary sub-regions B_2 and B_4 will also be equal.

3.2.4. Target detection probability of an SN placed in sub-region C_{I1}

The coverage area of an arbitrary SN positioned in sub-region C_{I1} is affected by side S_1 and S_2 of the RSR. In this case, the position of an SN denoted by $P(x, y)$ may have either of the two conditions *i.e.*, $x \le y$ or $x > y$. However, the mathematical composition for the probability of target position detection will remain the similar; hence, we assume a position of the SN with $x \le y$. The probability that a target is positioned at a location with a separation r to this arbitrary SN position is $2\pi r \times dr/A$, $r \in [0, x]$, $2r\left(\pi - cos^{-1}(x/r)\right) \times dr/A$, $r \in [x, y]$, and $2r\left(\pi - cos^{-1}(x/r) - cos^{-1}(y/r)\right) \times dr/A$, $r \in [y, r_{max}]$, where dr is a small variation in separation and can be computed with the help of Fig. 6. Therefore, the probability that the target would be sensed by this arbitrary SN is

$$\begin{aligned} P_{det}^{C_{I1}}(r) &= \int_0^x \phi\left(\frac{10\beta \log_{10}(r/\bar{r})}{\sigma}\right) \times \frac{2\pi r}{A}\,dr \\ &+ \int_x^y \phi\left(\frac{10\beta \log_{10}(r/\bar{r})}{\sigma}\right) \times \frac{2r\left(\pi - cos^{-1}(x/r)\right)}{A}\,dr \\ &+ \int_y^{r_{max}} \phi\left(\frac{10\beta \log_{10}(r/\bar{r})}{\sigma}\right) \\ &\times \frac{2r\left(\pi - cos^{-1}(x/r) - cos^{-1}(y/r)\right)}{A}\,dr \\ &= \int_0^{r_{max}} \phi\left(\frac{10\beta \log_{10}(r/\bar{r})}{\sigma}\right) \times \frac{2\pi r}{A}\,dr \\ &- \int_x^{r_{max}} \phi\left(\frac{10\beta \log_{10}(r/\bar{r})}{\sigma}\right) \times \frac{2r cos^{-1}(x/r)}{A}\,dr \\ &- \int_y^{r_{max}} \phi\left(\frac{10\beta \log_{10}(r/\bar{r})}{\sigma}\right) \times \frac{2r cos^{-1}(y/r)}{A}\,dr \end{aligned} \tag{42}$$

For an SN deployed in inner corner sub-regions C_{I1}, C_{I2}, C_{I3}, and C_{I4}, the probability that the target would be located at a position with a separation r to the SN location will be equal. Consequently, the probability that the target location will be sensed by an arbitrary SN deployed in either of the inner corner sub-region will also be equal.

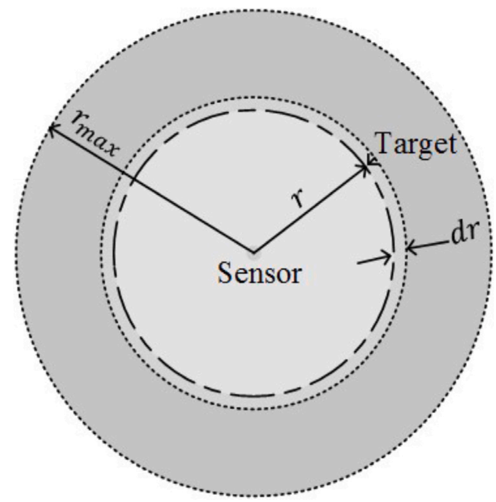

Fig. 5. Sensing range in shadowing environment.

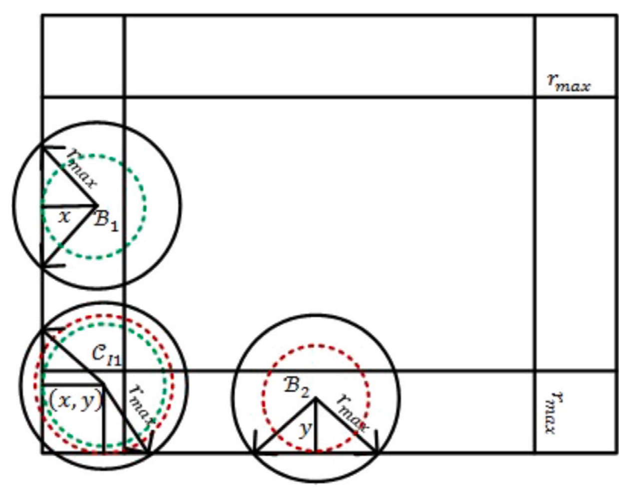

Fig. 6. Probability that the target is positioned at a point with distance r to the node lying in B_1, B_2, and C_{I1}.

3.2.5. Target detection probability of an SN placed in sub-region C_{O1}

The coverage area of an SN deployed at a position $P(x, y)$ in outer corner sub-region C_{O1} is influenced by sides S_1, S_2 and vertex V_1 of the RSR as shown in Fig. 7. For a given position of an SN in sub-region C_{O1}, we find two instances to compute the probability that the SN is positioned at a location with separation r to the target location and are discussed below:

- When $x \le y$, *i.e.*, $x \in \left(0, \frac{r_{max}}{\sqrt{2}}\right)$, $y \in \left(x, \sqrt{r_{max}^2 - x^2}\right)$
  In this case, the probabilities that an SN is deployed at a position with separation r to the target location is $2\pi r \times dr/A$, $r \in [0, x]$, $2r\left(\pi - cos^{-1}(x/r)\right) \times dr/A$, $r \in [x, y]$, and $r\left(1.5\pi - cos^{-1}(x/r) - cos^{-1}(y/r)\right) \times dr/A$, $r \in [y, r_{max}]$, where dr is a negligible difference in separation and can be computed with the help of Fig. 7. Therefore, the probability that a target position in shadowing environment will be sensed by an SN placed in

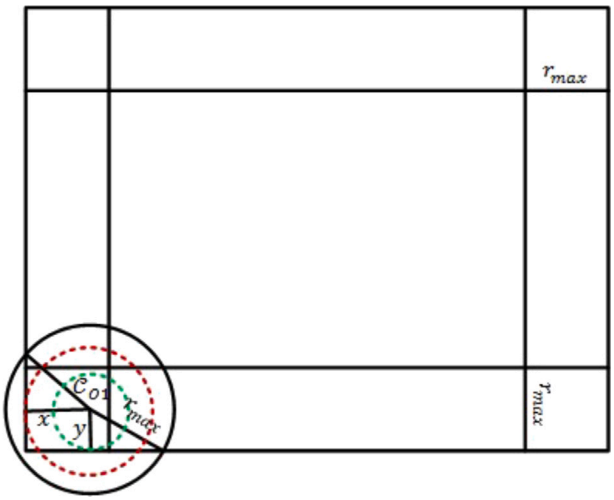

Fig. 7. Probability that the target is positioned at a point with distance r to the node lying in C_{O1}.

sub-region C_{O1} of the RSR is calculated as

$$
\begin{aligned}
P_{det}^{C_{O1}'}(r) = &\int_0^x \phi\left(\frac{10\beta\log_{10}(r/\bar{r})}{\sigma}\right) \times \frac{2\pi r}{A}\, dr \\
&+ \int_x^y \phi\left(\frac{10\beta\log_{10}(r/\bar{r})}{\sigma}\right) \times \frac{2r\left(\pi - cos^{-1}(x/r)\right)}{A}\, dr \\
&+ \int_y^{r_{max}} \phi\left(\frac{10\beta\log_{10}(r/\bar{r})}{\sigma}\right) \\
&\times \frac{r\left(1.5\pi - cos^{-1}(x/r) - cos^{-1}(y/r)\right)}{A}\, dr
\end{aligned}
\tag{43}
$$

- When $x > y$, *i.e.*, $x \in \left(0, \frac{r_{max}}{\sqrt{2}}\right), y \in (0, x)$
  Here, the probabilities that a target is positioned at a place with separation r to SN position in sub-region is $2\pi r \times dr/A$, $r \in [0, y]$, $2r\left(\pi - cos^{-1}(x/r)\right) \times dr/A$, $r \in [y, x]$, and $r\left(1.5\pi - cos^{-1}(x/r) - cos^{-1}(y/r)\right) \times dr/A$, $r \in [x, r_{max}]$, where dr is a tiny difference in separation can be computed with the help of Fig. 7. Thus, the probability that a target lying in shadowing environment will be sensed by an SN placed in this part of the sub-region C_{O1} is computed as

$$
\begin{aligned}
P_{det}^{C_{O1}''}(r) = &\int_0^y \phi\left(\frac{10\beta\log_{10}(r/\bar{r})}{\sigma}\right) \times \frac{2\pi r}{A}\, dr \\
&+ \int_y^x \phi\left(\frac{10\beta\log_{10}(r/\bar{r})}{\sigma}\right) \times \frac{2r\left(\pi - cos^{-1}(y/r)\right)}{A}\, dr \\
&+ \int_x^{r_{max}} \phi\left(\frac{10\beta\log_{10}(r/\bar{r})}{\sigma}\right) \\
&\times \frac{r\left(1.5\pi - cos^{-1}(x/r) - cos^{-1}(y/r)\right)}{A}\, dr
\end{aligned}
\tag{44}
$$

- When $x > y$, but $x \in \left(\frac{r_{max}}{\sqrt{2}}, r_{max}\right), y \in \left(0, \sqrt{r_{max}^2 - x^2}\right)$
  In this part, the probability of target position detection by an SN lying at a location with $x > y$ will be equal to $P^{C_{O1}''}$, but, the coordinates of the SN position in sub-region C_{O1} will follow the range $x \in \left(\frac{r_{max}}{\sqrt{2}}, r_{max}\right), y \in \left(0, \sqrt{r_{max}^2 - x^2}\right)$.
  For an SN placed in outer corner sub-regions C_{O1}, C_{O2}, C_{O3}, and C_{O4}, the probability that a target is positioned at a point with separation r to the SNs location will also be equal due to the same reason stated above. Consequently, the probability that the target location will be sensed by an SN deployed in either of the outer corner sub-region will also be equal.

Further, we average the target detection probability of an arbitrary SN over different sub-regions by incorporating BEs and SEs to evaluate the expected probability of target detection by an arbitrary SN deployed inside a RSR using Eq. (45)

$$
\begin{aligned}
E\left(P_{det}\right) = &\int_{r_{max}}^{w-r_{max}} \int_{r_{max}}^{l-r_{max}} \left(\frac{P_{det}^{I}(r)}{A}\right) dx\, dy \\
&+ 2\int_{r_{max}}^{w-r_{max}} \int_0^{r_{max}} \left(\frac{P_{det}^{B_1}(r)}{A}\right) dx\, dy \\
&+ 2\int_0^{r_{max}} \int_{r_{max}}^{l-r_{max}} \left(\frac{P_{det}^{B_2}(r)}{A}\right) dx\, dy \\
&+ 4\int_{\sqrt{r_{max}^2-x^2}}^{r_{max}} \int_0^{r_{max}} \left(\frac{P_{det}^{C_{I1}}(r)}{A}\right) dx\, dy \\
&+ 4\int_x^{\sqrt{r_{max}^2-x^2}} \int_0^{\frac{r_{max}}{\sqrt{2}}} \left(\frac{P_{det}^{C_{O1}'}(r)}{A}\right) dx\, dy \\
&+ 4\int_0^x \int_0^{\frac{r_{max}}{\sqrt{2}}} \left(\frac{P_{det}^{C_{O1}''}(r)}{A}\right) dx\, dy \\
&+ 4\int_0^{\sqrt{r_{max}^2-x^2}} \int_{\frac{r_{max}}{\sqrt{2}}}^{r_{max}} \left(\frac{P_{det}^{C_{O1}''}(r)}{A}\right) dx\, dy
\end{aligned}
\tag{45}
$$

3.3. Network k-coverage

Some of the major applications of WMNs are forest fire detection, monitoring of natural resource and border regions, enemy tracking, battlefield surveillance and reconnaissance (Roy, Mazumdar, & Pamula, 2021). The deployment of WMNs in the above mentioned regions is very expensive and cannot be modified after the initial deployment, therefore, it is important to estimate their performance before their actual deployment. The monitoring and surveillance performance of WMNs can be measured in terms of network coverage provided by the network (Boschiero, Giordani, Polese, & Zorzi, 2020; Chatterjee, Ghosh, & Das, 2017; Yu, Wan, Cheng, & Yu, 2017). Since, the SNs in a WMN may fail because of different reasons such as high winds, temperature variations, hitting by wild animals, battery-drainage, and several other environmental factors (Kaya, Keçeli, Catal, & Tekinerdogan, 2020; Shikada, Sebe, Suyama, & Indriawati, 2020), which in turn would deteriorate the network coverage. The impact of SNs failure on network coverage can be eliminated by designing a robust network against the SNs failure. A network is assumed to render k-coverage iff each location inside the region is sensed by no less than k different SNs. Hence, we compute the k-coverage of the WMN for both the cases, *i.e.*, with BEs only, and BEs plus SEs together. The probability that the target would not be detected by any arbitrary SN deployed inside the RSR is obtained as

$$
P_{ND} = \left(1 - E\left(P_{det}\right)\right)^N \tag{46}
$$

and the probability that the target would be sensed by an arbitrary SN is given by

$$
C_{Net} = 1 - P_{ND} = 1 - \left(1 - E\left(P_{det}\right)\right)^N \tag{47}
$$

Further, the probability that the target location is sensed by k different arbitrarily selected SNs from N is:

$$
P_k = \binom{N}{k} \left(E\left(P_{det}\right)\right)^k \left(1 - E\left(P_{det}\right)\right)^{N-k} \tag{48}
$$

and, the probability that the random target position in the RSR would be sensed by no less than k distinct arbitrary SNs can be

Table 1
Simulation parameters for k-barrier coverage probability.

Parameter	Value (s)
RSR	l = 100 – 1900 m and w = 35 – 1600 m
Maximum sensing range of SNs (r_{max})	(10 – 600) m
Number of SNs (N)	5 – 1500
Standard deviation of SEs (σ)	0 – 12dB
Value of required k	1 – 3

computed as

$$C_k = 1 - \sum_{k=0}^{k-1} P_k = 1 - \sum_{k=0}^{k-1} \binom{N}{k} \left(E\left(P_{det}\right)\right)^k \left(1 - E\left(P_{det}\right)\right)^{N-k} \tag{49}$$

The k-coverage probability of a WMN spread in RSR incorporating only BEs, and BEs plus SEs concurrently can be obtained by substituting Eqs. (38) and (45) respectively in Eq. (49).

3.4. Simulation set-up

To obtain the simulation results, the entire RSR is split into many similar squares with an area of 0.15 m × 0.15 m. The detection availability of every square is computed considering the similar topology in each round of iteration, and the square is presumed to be covered by the WMN iff its centre is sensed by at least one arbitrary SN (see Table 1).

Finally, the network coverage metric is computed as the ratio of squares covered to the total squares count. Also, the k-coverage probability of the WMN is achieved by implementing algorithms in MATLAB® 2018b. Each MCS result rendered is the average of 10000 iterations.

4. ML approach to predict network k-coverage

In this study, we employed supervised regression based ML approach, viz., GRNN. We have preferred explainable ML approach as compared to its black-box variant (Rudin, 2019).

4.1. Generalised regression neural networks

The GRNN is a radial basis function network that works on the principle of a standard statistical technique called kernel regression (Cigizoglu & Alp, 2006; Li, Guo, Li, & Sun, 2013). Donald F. Specht introduced GRNN in 1991 for the nonlinear regression analysis of continuous variables (Specht et al., 1991). GRNN has several features. For instance, it does not need any iterative training method to estimate a random function between input and output vectors. It can estimate the function directly from the training data. GRNN is much efficient than any other iterative training network in terms of time complexity. Besides, GRNN has better performance for learning speed and estimation capabilities. It converges to the optimal regression surface as the size of the training data set becomes vast. Furthermore, the evaluated error reaches zero with the increase in the size of the training set. GRNN also has acceptable prediction outcomes when the size of the training data is small.

GRNN is a technique to approximate the joint probability density function (pdf) of a vector random variable x and a scalar random variable y, denoted by $f(x, y)$. The conditional expected value of y given X is provided by Eq. (50)

$$E[y|X] = \frac{\int_{-\infty}^{\infty} y f(X, y) dy}{\int_{-\infty}^{\infty} f(X, y) dy} \tag{50}$$

where, X is a given computed value of vector random variable x, the value of the pdf $f(x, y)$ is estimated from the sample values of x and y when it is not available. Based on the sample values X^i and Y^i of the random variables x and y, the probability estimator $\hat{f}(X, Y)$ can be computed using Eq. (51)

$$\hat{f}(X, Y) = \frac{1}{(2\pi)^{(p+1)/2}\, \sigma^{(p+1)}} \frac{1}{n} \times \sum_{i=1}^{n} \exp\left[-\frac{\left(X - X^i\right)^T \left(X - X^i\right)}{2\sigma^2}\right] \exp\left[-\frac{\left(Y - Y^i\right)^2}{2\sigma^2}\right] \tag{51}$$

where, p represents the dimension of the vector variable x; n is the number of sample values; σ is the smoothing parameter indicating the capability of the GRNN. Scalar function D_i^2 is given by Eq. (52)

$$D_i^2 = \left(X - X^i\right)^T \left(X - X^i\right) \tag{52}$$

Putting Eq. (51) in Eq. (50) and evaluating the required interactions, we obtain Eq. (53) which can be applied directly to solve numerical data.

$$\hat{Y}(X) = \frac{\sum_{i=1}^{n} Y^i \exp\left(-\frac{D_i^2}{2\sigma^2}\right)}{\sum_{i=1}^{n} \exp\left(-\frac{D_i^2}{2\sigma^2}\right)} \tag{53}$$

Primarily, the GRNN is arranged in four layers, namely the input layer, pattern layer, summation layer, and output layer (Niu, Wang, Chen, & Liang, 2017) as depicted in Fig. 8. The function of each layer is described below:

1. **The input layer**: The number of inputs in this layer is equal to the number of variables under observation. In this layer, each input variable has one neuron. These neurons standardises the range of input variables by subtracting the median and diving by the interquartile range. Then the output of each neuron in the input layer is fed to the pattern layer.
2. **The pattern layer**: In this layer, a non-linear transformation is employed on the values obtained from the input layer. The transformation function of the ith neuron in the pattern layer is given by Eq. (54)

$$P_i = \exp\left[-\frac{D_i^2}{2\sigma^2}\right], i = 1, 2, 3, \dots, n \tag{54}$$

3. **The summation layer**: This layer possesses two types of neurons. The first neuron, denoted by S_A, computes the arithmetic addition of all the outcomes of the pattern layer neurons. The weight of connection for each neuron in the pattern layer to this neuron is 1. The transfer function of this neuron is given by Eq. (55)

$$S_A = \sum_{i=1}^{n} P_i \tag{55}$$

To create the additional neurons in the summation layer, denoted by S_{N_j}, the outputs of every neuron in the pattern layer were weighted and added. The following is the other neurons' transfer function in the summation layer:

$$S_{N_j} = \sum_{i=1}^{n} y_{ij} P_i j = 1, 2, \dots, k, \tag{56}$$

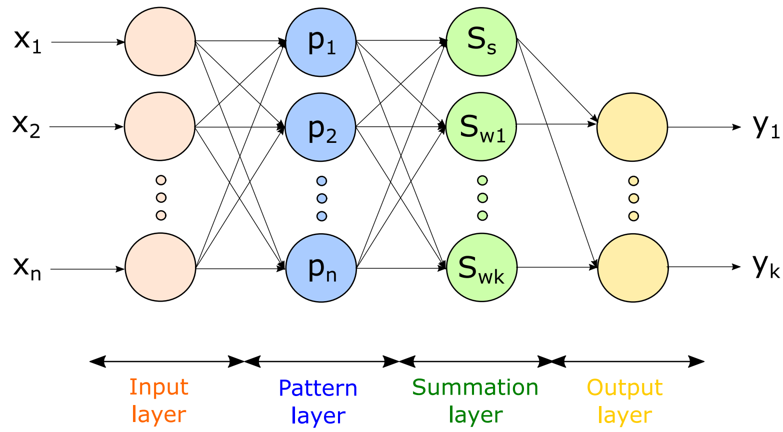

Fig. 8. Schematic architecture of GRNN.

where y_{ij} is the weight of the connection between the i_{th} pattern layer neuron and the j_{th} summation layer neuron. In more detail, y_{ij} is the j_{th} element in the i_{th} output sample.

4. **The output layer**: In this layer, the value accumulated in the numerator summation unit is divided by the denominator summation unit value, which is used as the predicted target value. The output of each neuron is:

$$y_j = \frac{S_{N_j}}{S_A}; j = 1, 2, \ldots, k, \tag{57}$$

where the j_{th} neuron's output is y_j.

The dimension of the complete datasets used is 136 × 7, the input features' dimensions are 136 × 6, and the output feature is 136 × 1. To train the GRNN model, we divided the entire data into a 80:20 ratio (Joseph, 2022; Singh, Amutha, Nagar, Sharma, & Lee, 2022a, 2022b). We used 105 × 6 data for training the model and the remaining to validate it. The number of neurons in the pattern layer usually equals or more than the number of training datasets. Hence, we consider 105 neurons in the pattern layer. Unlike with back-propagation networks, there are no training parameters like learning rate or momentum; nevertheless, a smoothing factor is used once the network has been trained. How closely the network predicted values match with the data in the training patterns depends on the smoothing factor. We observe that a unity smoothing factor converges the network faster than other values of this factor.

4.2. Assessing the features importance and sensitivity

It is well-known that the performance of an ML approach can greatly be influenced by the choice of features inputs. The relative importance of identified features on the predicand is assessed by employing the regression ensemble technique proposed in Singh, Kotiyal, et al. (2020), Singh, Nagar, et al. (2021). In this study, the key input features selected are length, breadth, SNs, sensing range, sigma, and required k to predict the k-coverage probability as the predictand. The relative importance charts both for with/without BE are depicted in Fig. 9. It can be observed from Fig. 9(a) that in without BEs the relative importance score of sensing range is highest (followed by length, breadth, required k, and nodes, respectively) whereas with BEs (Fig. 9(b)), the relative importance of sensing range is the highest (followed by length, required k, breadth and nodes). However, in both the cases, sigma gets the least importance.

Notwithstanding that feature importance just says us about the relative importance of each feature based on the training datasets, but it does not convey any information on how the feature is related to the predictand *i.e.,* whether the feature has a positive or negative impact on the prediction (Singh, Gaurav, et al., 2021). To evaluate the second aspect, performed the sensitivity analysis of the features using Partial Dependence Plot (PDP) and Individual Conditional Expectation (ICE) curve by leveraging regression tree ensemble learning (Singh & Gaurav, 2023; Singh et al., 2023). Figs. 10 and 11 show the results of sensitivity analysis. Note that the PDP curve (shown in red) measures the average effect of each feature by marginalising all other features. In contrast, ICE curves (shown in grey) dis-aggregates the average effect and presents the functional relationship at each instant.

It can be seen that the length, breadth, sigma, and required k has a negative and SNs and sensing range has a positive impact on the predictand for both with and without BEs scenarios. The value of k-coverage probability decreases with increase in length, breadth, sigma, and required k, whereas it increases with increase in sensing range and SN's count.

5. Results

Here, we discuss the performance of GRNN in predicting the k-coverage probability. We plot a linear regression curve and the corresponding residual plot for the two scenarios (*i.e.,* with and without BEs). We assess the GRNN algorithm's performance using three performance metrics: bias, RMSE, and coefficient of correlation (R).

5.1. Without BEs

After obtaining the predicted k-coverage probability (with out BEs) from the trained GRNN algorithm, we have compared its results with the observed values obtained through MCS. To do this, we created a linear regression line (Fig. 12) between the observed and anticipated values. With R = 0.78 and RMSE = 0.15, we found that the results match the observed values quite well. However, this model produces a small positive bias of 0.02 which results in a slight overestimation of few samples as illustrated in Fig. 12.

Further, to assess the appropriateness of the ML approach, we performed and plotted the residual analysis curve between the predicted and observed values of k-coverage probability (Fig. 13). The residual plot is randomly scattered without following any periodic pattern indicating a good fit. The positive residual above the RMSE dash-line represents an overestimation greater than the RMSE value. Similarly, the negative residual value below the dash-line represents an underestimation greater than the RMSE value. The positive bias represents that the positive residual is more than the negative residual.

5.2. With BEs

In this sub-section, we assess the effectiveness of GRNN for with BEs case. In doing so, we compare the predicted results of GRNN algorithm

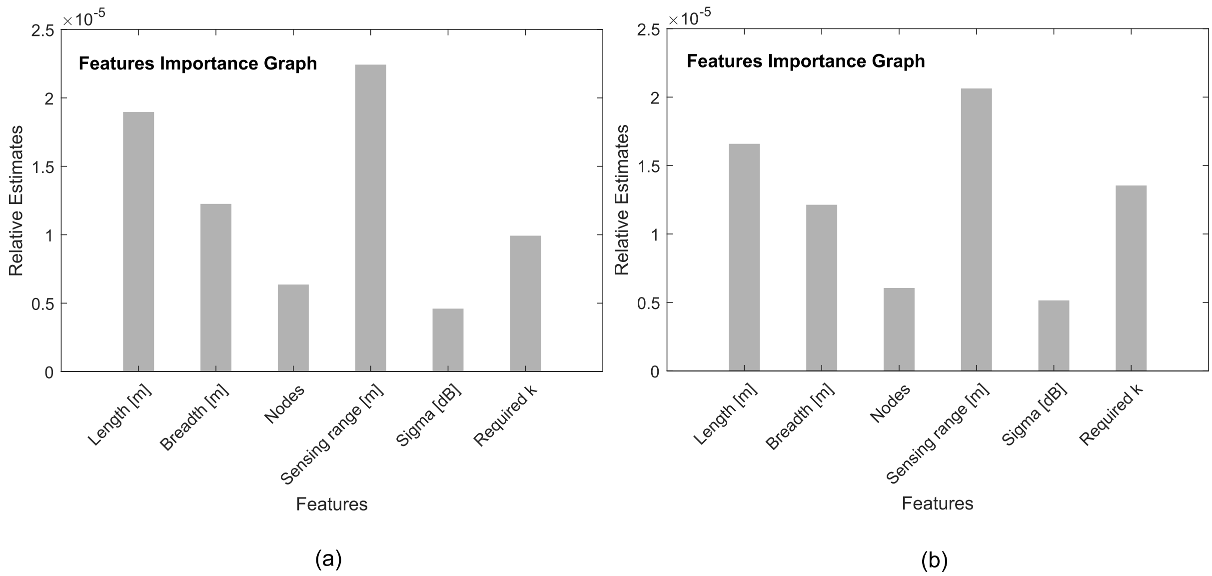

Fig. 9. Feature importance graph illustrating the relative importance of each features for (a) without BEs and (b) with BEs.

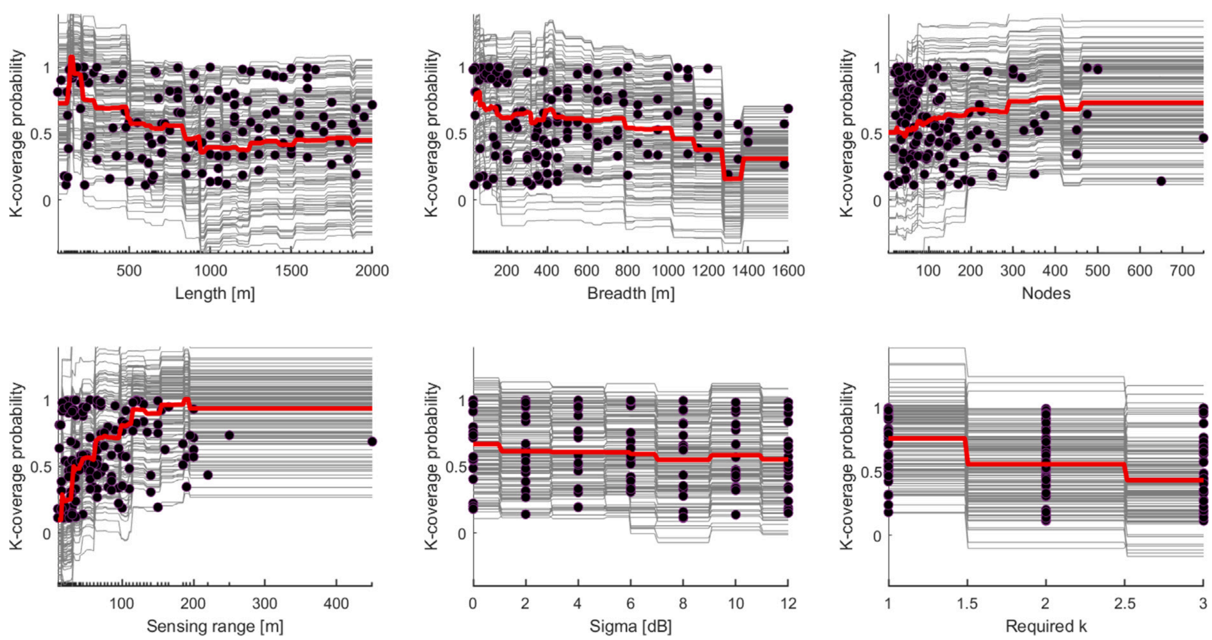

Fig. 10. Sensitivity analysis of each features using Partial Dependence Plot (PDP) (in red) and Individual Conditional Expectation (ICE) curve (in grey) for no BEs scenario.

with the simulated results obtained from MCS. We plot a regression line between the GRNN predicted and simulated observed values (Fig. 14). We observed that the data points lie along the regression line with R = 0.78 and RMSE = 0.14 similar to the case of without BEs. In this case also, we observed that the approach persist a small bias of 0.02 which leads to overestimation of few sample points as shown in Fig. 14.

Similar to the case of without BEs, the residuals in the residual analysis curve (Fig. 15) does not follows any specific pattern and hence represents a good fit line. Furthermore, the presence of positive bias confirms that the total positive residual is greater than the total negative residual.

6. Discussion

This study uses GRNN ML model to predict the *k*-coverage probability for two different scenarios in WSNs; with and without BEs. Our results suggest that the performance of GRNN is nearly similar for both these scenarios with slightly good performance (in terms of RMSE) for with BEs scenario.

Further, to ensure fair evaluation, we also compare the outputs of GRNN with other benchmark algorithms (Table 2). For this, we selected bagging ensemble learning and boosting ensemble learning (Sagi & Rokach, 2018). In doing so, we choose R, RMSE, bias and time complexity as the performance metrics. We observed that GRNN approach outperforms both the algorithms. Also, we observed no obvious difference in the time-complexity in with and without boundary effect scenarios for each individual algorithms. GRNN emerges as most accurate (lowest RMSE) and time efficient algorithm followed by bagging ensemble learning and boosting ensemble learning in predicting the *k*-coverage probability.

Furthermore, we evaluate and compare the computational time complexity of all the three ML algorithms with three different scenarios of MCS. We calculate the computational time for SN 50, 100, and 150

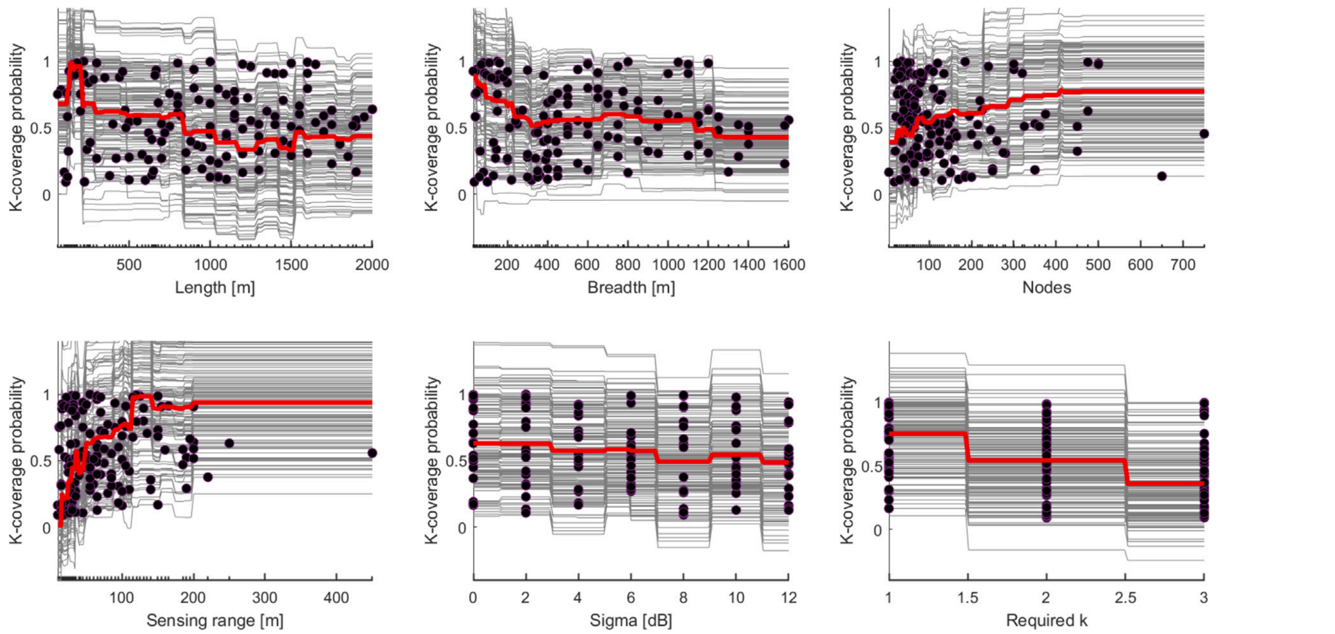

Fig. 11. Sensitivity analysis of each features using Partial Dependence Plot (PDP) (in red) and Individual Conditional Expectation (ICE) curve (in grey) for with BEs scenario.

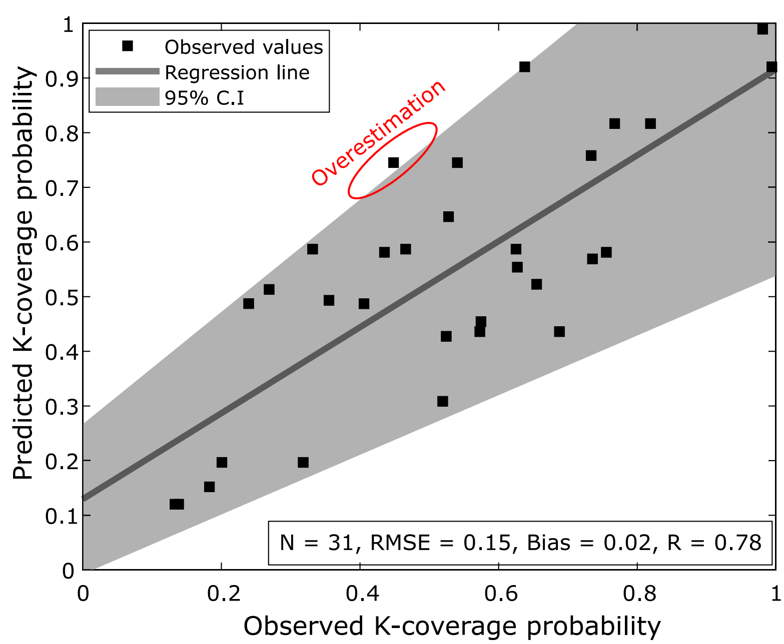

Fig. 12. Comparison between the observed and predicted values of k-coverage probability without considering BEs. The grey band represents 95% confidence interval.

Table 2
Simulation parameters for k-barrier coverage probability.

Metrics	Methods					
	GRNN		Bragging Ensemble Learning		Boosting Ensemble Learning	
	with BEs	without BEs	with BEs	without BEs	with BEs	without BEs
R	0.78	0.78	0.63	0.59	0.67	0.51
RMSE	0.14	0.15	0.17	0.19	0.17	0.20
Bias	0.02	0.02	0.05	0.04	−0.04	0.01
Time (s)	0.71	0.76	1.25	1.23	1.00	1.05

by keeping all other parameters constant (r_{max} = 30 m, σ = 2 dB, fading factor, β = 4) for 10e3 iterations in 100 m × 80 m. In doing so, we observed that the GRNN algorithm is the most time-efficient ML algorithm for predicting k-coverage probability. However the differences in the computational time of all the ML algorithms are not significant. Further, the difference in the time-complexity of all the three ML algorithms becomes negligible when it is compared with the time complexity involve in the simulations. Furthermore, we observed

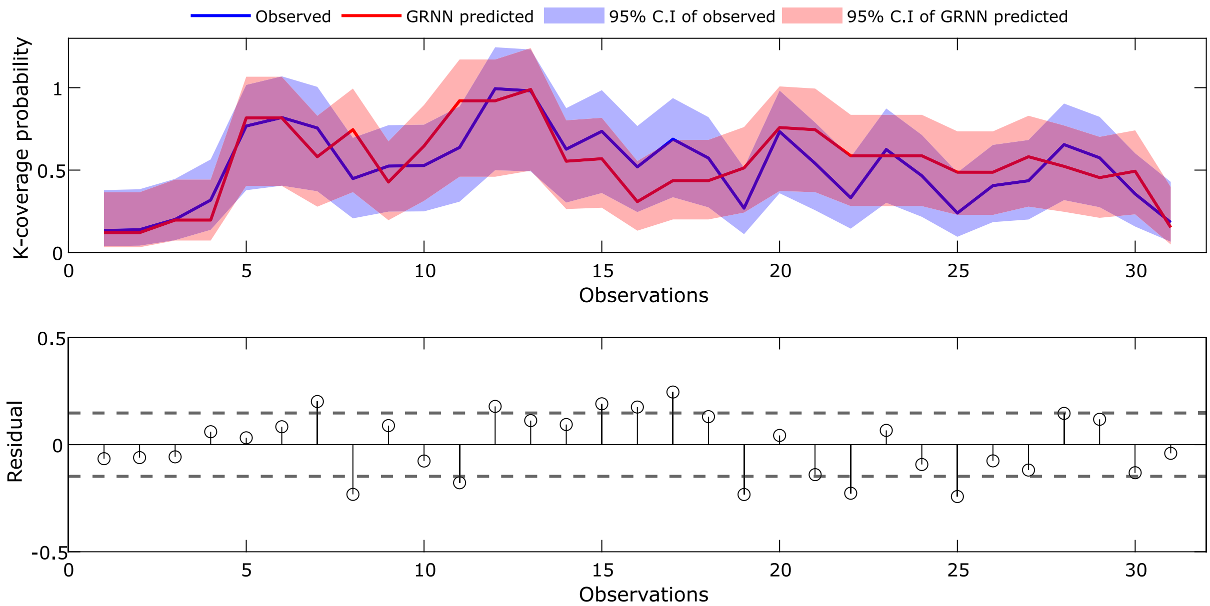

Fig. 13. Residual plot analysis of k-coverage probability without considering BEs. The dash-line in the figure is the RMSE.

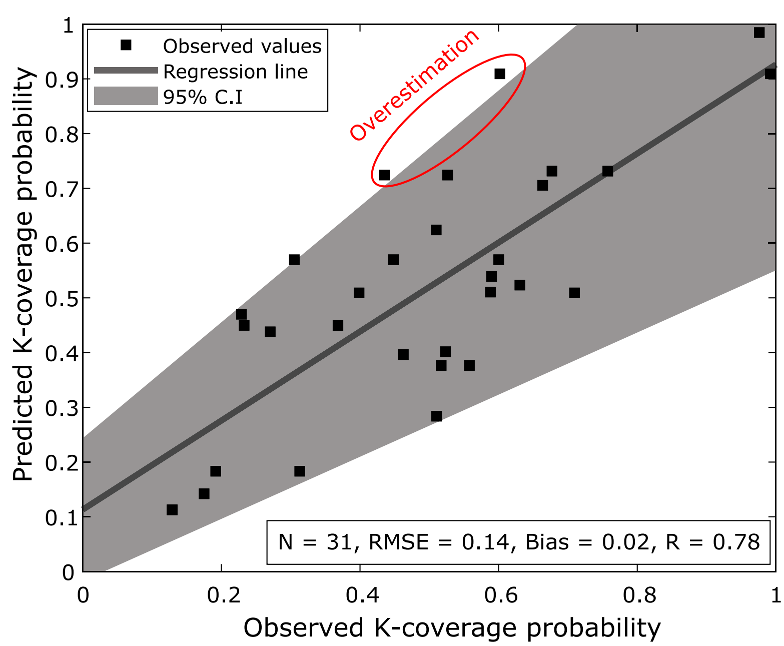

Fig. 14. Comparison between the observed and predicted values of k-coverage probability with BEs. The grey band represents 95% confidence interval.

that the time-complexity for the simulation scenario rises with increase in the number of SNs (Fig. 16).

The limitation of the proposed study is that it is limited to an RSR only. This study can be generalised for any geometrical-shaped region considering area as the feature instead of length and breadth separately. However, for an RSR, the k-coverage probability has independent dependency on length and breadth (Nze et al., 2011) which was indeed the motivation behind selecting length and breadth as separate features in this study.

7. Conclusion

In this study, we rendered and investigated a comprehensive approach to accurately estimate k-barrier coverage probability using ML algorithms. We evaluated and compared the performance of three different ML algorithms, namely GRNN, bagging ensemble learning and boosting ensemble learning. We trained these ML model using length, breadth, SNs, sensing range, sigma value, and required k as potential features. In doing so, we have shown that sensing range is a pivotal feature for predicting k-coverage probability. Further, GRNN outperforms the other two algorithms in terms of accuracy and time complexity. This is probably because the former has less number of hyperparameters as compared to the other two algorithms which prevents GRNN from getting trapped into local minima.

This study is a step towards predicting k-coverage probability using various system parameters. Our first-order analysis can be used to cut down the time requirements during and post network set-up.

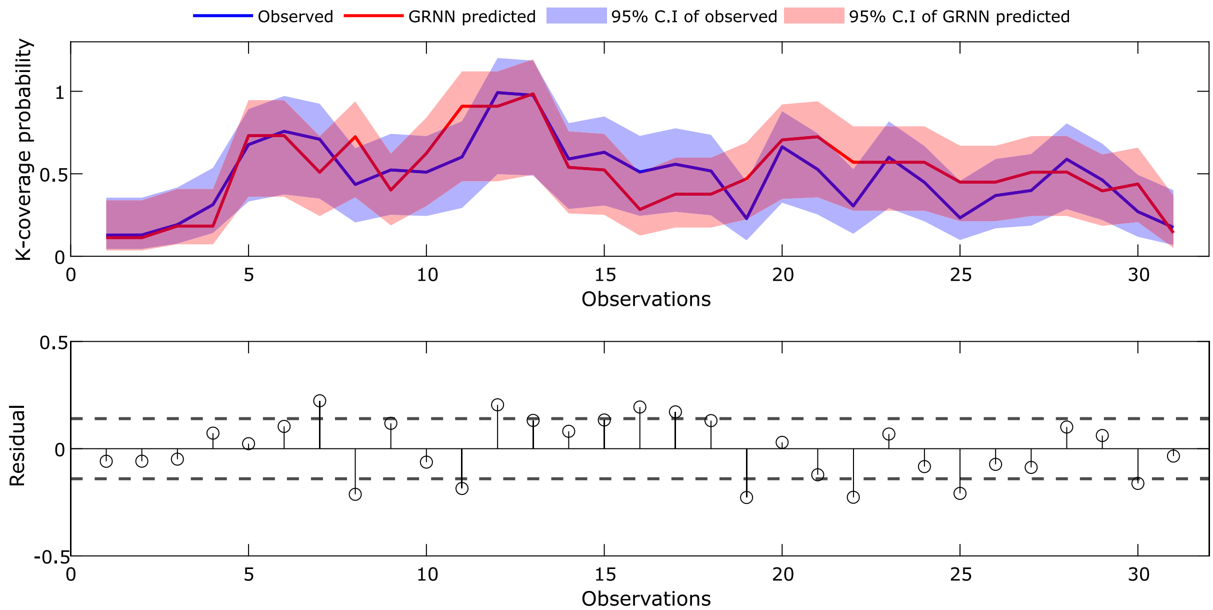

Fig. 15. Residual plot analysis of k-coverage probability with BEs. The dash-line in the figure is the RMSE.

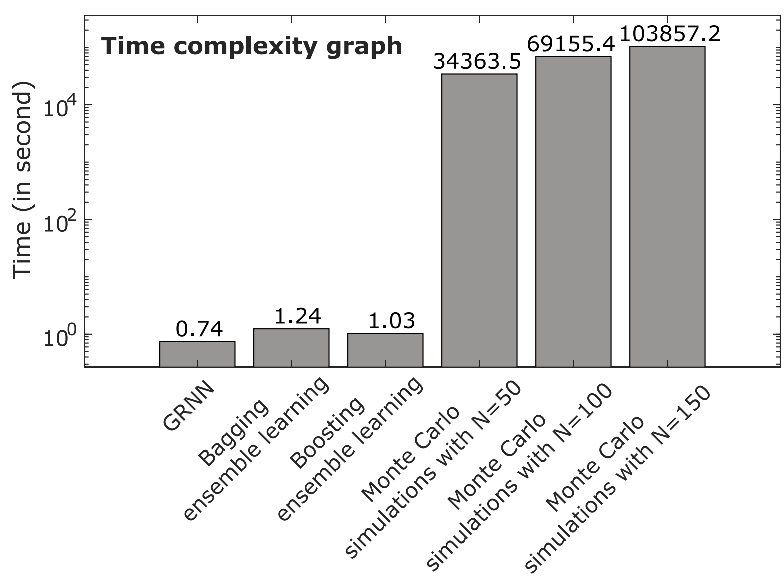

Fig. 16. Computational time complexity comparison graph. The y-axis is in log-scale.

Code availability

The code and data used in this study will be made publicly available post acceptance of this manuscript and on request from a reader as well.

CRediT authorship contribution statement

Jaiprakash Nagar: Conceptualisation, Methodology, Software, Data curation, Validation, Analysis, Writing – original draft, Visualization, Investigation, Writing – review & editing. **Sanjay Kumar Chaturvedi:** Methodology, Visualization, Writing – review & editing, Supervision. **Sieteng Soh:** Visualization, Investigation, Writing – review & editing, Supervision. **Abhilash Singh:** Methodology, Software, Writing – original draft, Validation, Analysis, Writing – review & editing.

Declaration of competing interest

The authors declare that they have no known competing financial interests or personal relationships that could have appeared to influence the work reported in this paper.

Data availability

Data will be made available on request.

Acknowledgements

We would like to acknowledge IIT Kharagpur, Curtin University Australia, and IISER Bhopal, for providing institutional support.

References

Afshang, M., & Dhillon, H. S. (2017). Fundamentals of modeling finite wireless networks using binomial point process. *IEEE Transactions on Wireless Communication*, *16*(5), 3355–3370.

Al-Turjman, F. M., Hassanein, H. S., & Ibnkahla, M. (2013). Quantifying connectivity in wireless sensor networks with grid-based deployments. *Journal of Network and Computer Applications*, *36*(1), 368–377.

Alam, K. M., Kamruzzaman, J., Karmakar, G., & Murshed, M. (2014). Dynamic adjustment of sensing range for event coverage in wireless sensor networks. *Journal of Network and Computer Applications*, *46*, 139–153.

Albert, R., & Barabási, A.-L. (2002). Statistical mechanics of complex networks. *Reviews of Modern Physics*, *74*(1), 47.

Ali, S., Saad, W., Rajatheva, N., Chang, K., Steinbach, D., Sliwa, B., et al. (2020). 6G white paper on machine learning in wireless communication networks. arXiv preprint arXiv:2004.13875.

Alsheikh, M. A., Lin, S., Niyato, D., & Tan, H.-P. (2014). Machine learning in wireless sensor networks: Algorithms, strategies, and applications. *IEEE Communications Surveys & Tutorials*, *16*(4), 1996–2018.

Amutha, J., Nagar, J., & Sharma, S. (2021). A distributed border surveillance (dbs) system for rectangular and circular region of interest with wireless sensor networks in shadowed environments. *Wireless Personal Communications*, *117*(3), 2135–2155.

Amutha, J., Sharma, S., & Nagar, J. (2020). WSN strategies based on sensors, deployment, sensing models, coverage and energy efficiency: Review, approaches and open issues. *Wireless Personal Communications*, *111*(2), 1089–1115.

Amutha, J., Sharma, S., & Sharma, S. K. (2021). Strategies based on various aspects of clustering in wireless sensor networks using classical, optimization and machine learning techniques: Review, taxonomy, research findings, challenges and future directions. *Computer Science Review*, *40*, Article 100376.

Arora, M., & Pal, A. (2022). A deep learning approach to accurately predict the κ-coverage probability in wireless sensor networks. *Wireless Personal Communications*, 1–18.

Boschiero, M., Giordani, M., Polese, M., & Zorzi, M. (2020). Coverage analysis of UAVs in millimeter wave networks: A stochastic geometry approach. In *2020 international wireless communications and mobile computing* (pp. 351–357). IEEE.

Brust, M. R., Ribeiro, C. H., & Barbosa Filho, J. A. (2009). Border effects in the simulation of ad hoc and sensor networks. In *2009 11th international conference on computer modelling and simulation* (pp. 180–185). IEEE.

Chatterjee, P., Ghosh, S. C., & Das, N. (2017). Load balanced coverage with graded node deployment in wireless sensor networks. *IEEE Transactions on Multi-Scale Computing Systems*, *3*(2), 100–112.

Chen, M., Challita, U., Saad, W., Yin, C., & Debbah, M. (2019). Artificial neural networks-based machine learning for wireless networks: A tutorial. *IEEE Communications Surveys & Tutorials*, *21*(4), 3039–3071.

Chowdhury, R., Rahman, M. A., Rahman, M. S., & Mahdy, M. (2020). An approach to predict and forecast the price of constituents and index of cryptocurrency using machine learning. *Physica A: Statistical Mechanics and its Applications*, *551*, Article 124569.

Cigizoglu, H. K., & Alp, M. (2006). Generalized regression neural network in modelling river sediment yield. *Advances in Engineering Software*, *37*(2), 63–68.

Dalveren, Y., & Ali, K. (2020). Performance evaluation of empirical path loss models for a linear wireless sensor network deployment in suburban and rural environments. *Hittite Journal of Science and Engineering*, *7*(4), 313–320.

Debnath, S., & Hossain, A. (2019). Network coverage in interference limited wireless sensor networks. *Wireless Personal Communications*, *109*(1), 139–153.

Dreifuerst, R. M., Daulton, S., Qian, Y., Varkey, P., Balandat, M., Kasturia, S., et al. (2021). Optimizing coverage and capacity in cellular networks using machine learning. In *ICASSP 2021-2021 IEEE international conference on acoustics, speech and signal processing* (pp. 8138–8142). IEEE.

Du, J., Jiang, C., Wang, J., Ren, Y., & Debbah, M. (2020). Machine learning for 6G wireless networks: Carrying forward enhanced bandwidth, massive access, and ultrareliable/low-latency service. *IEEE Vehicular Technology Magazine*, *15*(4), 122–134.

Fadoul, M. M. (2020). Rate and coverage analysis in multi-tier heterogeneous network using stochastic geometry approach. *Ad Hoc Networks*, *98*, Article 102038.

Fernandes, D. F., Raimundo, A., Cercas, F., Sebastião, P. J., Dinis, R., & Ferreira, L. S. (2020). Comparison of artificial intelligence and semi-empirical methodologies for estimation of coverage in mobile networks. *IEEE Access*, *8*, 139803–139812.

Fourati, H., Maaloul, R., & Chaari, L. (2021). A survey of 5G network systems: challenges and machine learning approaches. *International Journal of Machine Learning and Cybernetics*, *12*(2), 385–431.

Gupta, H. P., Rao, S. V., & Venkatesh, T. (2014). Critical sensor density for partial coverage under border effects in wireless sensor networks. *IEEE Transactions on Wireless Communication*, *13*(5), 2374–2382.

Habibiyan, R., & Sabbagh, A. G. (2022). Connectivity analysis of 2D underwater optical wireless sensor networks using a geometric approach. *Ad Hoc Networks*, *134*, Article 102910.

Han, G., Jiang, J., Zhang, C., Duong, T. Q., Guizani, M., & Karagiannidis, G. K. (2016). A survey on mobile anchor node assisted localization in wireless sensor networks. *IEEE Communications Surveys & Tutorials*, *18*(3), 2220–2243.

Hechmi, J. M., Zrelli, A., Kbida, M., Khlaifi, H., & Ezzedine, T. (2018). Coverage and connectivity of WSN models for health open-pit mines monitoring. In *2018 14th international wireless communications & mobile computing conference* (pp. 310–315). IEEE.

Ide, C., Hadiji, F., Habel, L., Molina, A., Zaksek, T., Schreckenberg, M., et al. (2015). LTE connectivity and vehicular traffic prediction based on machine learning approaches. In *2015 IEEE 82nd vehicular technology conference* (pp. 1–5). IEEE.

Jeong, Y.-S., & Sim, S.-H. (2021). Hierarchical multipath blockchain based IoT information management techniques for efficient distributed processing of intelligent IoT information. *Sensors*, *21*(6), 2049.

Jiang, C., Zhang, H., Ren, Y., Han, Z., Chen, K.-C., & Hanzo, L. (2016). Machine learning paradigms for next-generation wireless networks. *IEEE Wireless Communications*, *24*(2), 98–105.

Jo, H.-S., Park, C., Lee, E., Choi, H. K., & Park, J. (2020). Path loss prediction based on machine learning techniques: Principal component analysis, artificial neural network, and Gaussian process. *Sensors*, *20*(7), 1927.

Jondhale, S. R., & Deshpande, R. S. (2018). Kalman filtering framework-based real time target tracking in wireless sensor networks using generalized regression neural networks. *IEEE Sensors Journal*, *19*(1), 224–233.

Jondhale, S. R., & Deshpande, R. S. (2019). Efficient localization of target in large scale farmland using generalized regression neural network. *International Journal of Communication Systems*, *32*(16), Article e4120.

Joseph, V. R. (2022). Optimal ratio for data splitting. *Statistical Analysis and Data Mining: The ASA Data Science Journal*, *15*(4), 531–538.

Kamel, A. H., Afan, H. A., Sherif, M., Ahmed, A. N., & El-Shafie, A. (2021). RBFNN versus GRNN modeling approach for sub-surface evaporation rate prediction in arid region. *Sustainable Computing: Informatics and Systems*, *30*, Article 100514.

Kandris, D., Nakas, C., Vomvas, D., & Koulouras, G. (2020). Applications of wireless sensor networks: an up-to-date survey. *Applied System Innovation*, *3*(1), 14.

Kang, M.-J., & Kang, J.-W. (2016). A novel intrusion detection method using deep neural network for in-vehicle network security. In *2016 IEEE 83rd vehicular technology conference* (pp. 1–5). IEEE.

Katti, A. (2022). Target coverage in random wireless sensor networks using cover sets. *Journal of King Saud University-Computer and Information Sciences*, *34*(3), 734–746.

Kaya, A., Keçeli, A. S., Catal, C., & Tekinerdogan, B. (2020). Sensor failure tolerable machine learning-based food quality prediction model. *Sensors*, *20*(11), 3173.

Khalid, Z., & Durrani, S. (2013). Distance distributions in regular polygons. *IEEE Transactions on Vehicular Technology*, *62*(5), 2363–2368.

Kotiyal, V., Singh, A., Sharma, S., Nagar, J., & Lee, C.-C. (2021). ECS-NL: An enhanced cuckoo search algorithm for node localisation in wireless sensor networks. *Sensors*, *21*(11), http://dx.doi.org/10.3390/s21113576, URL: https://www.mdpi.com/1424-8220/21/11/3576.

Kumar, D. P., Amgoth, T., & Annavarapu, C. S. R. (2019). Machine learning algorithms for wireless sensor networks: A survey. *Information Fusion*, *49*, 1–25.

Laranjeira, L. A., & Rodrigues, G. N. (2014). Border effect analysis for reliability assurance and continuous connectivity of wireless sensor networks in the presence of sensor failures. *IEEE Transactions on Wireless Communication*, *13*(8), 4232–4246.

Li, H.-z., Guo, S., Li, C.-j., & Sun, J.-q. (2013). A hybrid annual power load forecasting model based on generalized regression neural network with fruit fly optimization algorithm. *Knowledge-Based Systems*, *37*, 378–387.

Liu, Z., Jia, W., & Wang, G. (2018). Area coverage estimation model for directional sensor networks. *International Journal of Embedded Systems*, *10*(1), 13–21.

Mahfouz, S., Mourad-Chehade, F., Honeine, P., Farah, J., & Snoussi, H. (2014). Target tracking using machine learning and Kalman filter in wireless sensor networks. *IEEE Sensors Journal*, *14*(10), 3715–3725.

Mamun, Q., Islam, R., & Kaosar, M. (2014). Anomaly detection in wireless sensor network. *Journal of Networks*, *9*(11), 2914.

Miao, Q., Huang, B., & Jia, B. (2020). Estimating distances via received signal strength and connectivity in wireless sensor networks. *Wireless Networks*, *26*(2), 971–982.

Mohammadjafari, S., Roginsky, S., Kavurmacioglu, E., Cevik, M., Ethier, J., & Bener, A. B. (2020). Machine learning-based radio coverage prediction in urban environments. *IEEE Transactions on Network and Service Management*, *17*(4), 2117–2130.

Nagar, J., Chaturvedi, S. K., & Soh, S. (2020a). An analytical model to estimate the performance metrics of a finite multihop network deployed in a rectangular region. *Journal of Network and Computer Applications*, *149*, Article 102466.

Nagar, J., Chaturvedi, S. K., & Soh, S. (2020b). Connectivity analysis of finite wireless multihop networks incorporating boundary effects in shadowing environments. *IET Communications*.

Nayak, P., Swetha, G., Gupta, S., & Madhavi, K. (2021). Routing in wireless sensor networks using machine learning techniques: Challenges and opportunities. *Measurement*, *178*, Article 108974.

Niu, D., Wang, H., Chen, H., & Liang, Y. (2017). The general regression neural network based on the fruit fly optimization algorithm and the data inconsistency rate for transmission line icing prediction. *Energies*, *10*(12), 2066.

Nze, G.-C. A., Guinand, F., & Pigne, Y. (2011). Impact of square environment on the connectivity in finite ad hoc networks. In *2011 the 14th international symposium on wireless personal multimedia communications* (pp. 1–5). IEEE.

Pal, A., et al. (2022). Coverage sensitivity analysis of a wireless sensor network with different sensing range models considering boundary effects. *Materials Today: Proceedings*, *49*, 3640–3645.

Rahman, M. S., Park, Y., & Kim, K.-D. (2012). RSS-based indoor localization algorithm for wireless sensor network using generalized regression neural network. *Arabian Journal for Science and Engineering*, *37*(4), 1043–1053.

Roy, S., Mazumdar, N., & Pamula, R. (2021). An energy and coverage sensitive approach to hierarchical data collection for mobile sink based wireless sensor networks. *Journal of Ambient Intelligence and Humanized Computing*, *12*(1), 1267–1291.

Rudin, C. (2019). Stop explaining black box machine learning models for high stakes decisions and use interpretable models instead. *Nature Machine Intelligence*, *1*(5), 206–215.

Sagi, O., & Rokach, L. (2018). Ensemble learning: A survey. *Wiley Interdisciplinary Reviews: Data Mining and Knowledge Discovery*, *8*(4), Article e1249.

Seferagić, A., Famaey, J., De Poorter, E., & Hoebeke, J. (2020). Survey on wireless technology trade-offs for the industrial internet of things. *Sensors*, *20*(2), 488.

Sharma, H., Haque, A., & Blaabjerg, F. (2021). Machine learning in wireless sensor networks for smart cities: A survey. *Electronics*, *10*(9), 1012.

Sharma, S., & Nagar, J. (2020). Intrusion detection in mobile sensor networks: A case study for different intrusion paths. *Wireless Personal Communications*, *115*(3), 2569–2589.

Shikada, K., Sebe, N., Suyama, K., & Indriawati, K. (2020). Robust fault-tolerant servo system against sensor failure and plant uncertainties. In *2020 59th annual conference of the Society of Instrument and Control Engineers of Japan* (pp. 1886–1981). IEEE.

Singh, A., Amutha, J., Nagar, J., Sharma, S., & Lee, C.-C. (2022a). AutoML-ID: Automated machine learning model for intrusion detection using wireless sensor network. *Scientific Reports*, *12*(1), 9074.

Singh, A., Amutha, J., Nagar, J., Sharma, S., & Lee, C.-C. (2022b). Lt-fs-id: Log-transformed feature learning and feature-scaling-based machine learning algorithms to predict the k-barriers for intrusion detection using wireless sensor network. *Sensors*, *22*(3), 1070.

Singh, A., & Gaurav, K. (2023). Deep learning and data fusion to estimate surface soil moisture from multi-sensor satellite images. *Scientific Reports*, *13*(1), 2251.

Singh, A., Gaurav, K., Meena, G. K., & Kumar, S. (2020). Estimation of soil moisture applying modified dubois model to Sentinel-1; a regional study from central India. *Remote Sensing*, *12*(14), 2266.

Singh, A., Gaurav, K., Rai, A. K., & Beg, Z. (2021). Machine learning to estimate surface roughness from satellite images. *Remote Sensing*, *13*(19), 3794.

Singh, A., Kotiyal, V., Sharma, S., Nagar, J., & Lee, C.-C. (2020). A machine learning approach to predict the average localization error with applications to wireless sensor networks. *IEEE Access*, *8*, 208253–208263.

Singh, A., Mehra, M., Kumar, A., Niranjannaik, M., Priya, D., & Gaurav, K. (2023). Leveraging hybrid machine learning and data fusion for accurate mapping of malaria cases using meteorological variables in western India. *Intelligent Systems with Applications*, *17*, Article 200164.

Singh, A., Nagar, J., Sharma, S., & Kotiyal, V. (2021). A Gaussian process regression approach to predict the k-barrier coverage probability for intrusion detection in wireless sensor networks. *Expert Systems with Applications*, *172*, Article 114603.

Singh, A., Sharma, S., & Singh, J. (2021). Nature-inspired algorithms for wireless sensor networks: A comprehensive survey. *Computer Science Review*, *39*, Article 100342.

Specht, D. F., et al. (1991). A general regression neural network. *IEEE Transactions on Neural Networks*, *2*(6), 568–576.

Stern, R. E., Song, J., & Work, D. B. (2017). Accelerated Monte Carlo system reliability analysis through machine-learning-based surrogate models of network connectivity. *Reliability Engineering & System Safety*, *164*, 1–9.

Stoyanova, M., Nikoloudakis, Y., Panagiotakis, S., Pallis, E., & Markakis, E. K. (2020). A survey on the internet of things (IoT) forensics: challenges, approaches, and open issues. *IEEE Communications Surveys & Tutorials*, *22*(2), 1191–1221.

Tan, X., Su, S., Huang, Z., Guo, X., Zuo, Z., Sun, X., et al. (2019). Wireless sensor networks intrusion detection based on SMOTE and the random forest algorithm. *Sensors*, *19*(1), 203.

Tsai, Y.-R. (2008). Sensing coverage for randomly distributed wireless sensor networks in shadowed environments. *IEEE Transactions on Vehicular Technology*, *57*(1), 556–564.

Vijayakumar, V., & Balakrishnan, N. (2021). Artificial intelligence-based agriculture automated monitoring systems using WSN. *Journal of Ambient Intelligence and Humanized Computing*, 1–8.

Xu, X., & Lin, J. C.-W. (2023). Abnormal nodes sensing model in regional wireless networks based on convolutional neural network. *Wireless Networks*, 1–12.

Yu, J., Wan, S., Cheng, X., & Yu, D. (2017). Coverage contribution area based k-coverage for wireless sensor networks. *IEEE Transactions on Vehicular Technology*, *66*(9), 8510–8523.